AN ABSTRACT OF THE THESIS OF

Lisa Andes for the degree of Master of Ocean Engineering in Ocean Engineering presented on June 19, 2007.

Title: Wave Propagation Processes at the Mouth of the Columbia River

Abstract approved:

H. Tuba Özkan-Haller

The mouth of the Columbia River (MCR) has a longstanding reputation of hazardous navigational conditions. This reputation has been developing since the first ship, the Columbia, traversed through the inlet in 1792. The hazardous conditions are related to the large waves and strong tidal currents that are common in the area. Tidal currents often reach 2 m/s. As large waves interact with strong tidal currents waves can steepen and break. This study investigates on the importance of wave-current interaction at the MCR. To model these conditions a two dimensional spectral model, SWAN (Simulating WAves Nearshore) (Booij, 1999), was used. SWAN simulations were completed neglecting as well as including current to make comparisons. Wave height and length were found to be influenced considerably by wave-current interaction.

The SWAN simulations were also compared to both radar and insitu observations. Radar–estimated and SWAN–predicted wave direction and wave breaking were compared. SWAN-predicted wave direction and radar-observed wave direction compared well; however, poor agreement between observations and predictions occurred over a

shoal in the region used to make comparisons. The source of this disagreement is unknown. Radar–observed wave breaking compared well with SWAN-predicted wave breaking in depth-limited cases; however, radar-observations indicate current induced wave breaking that SWAN does not predict. Insitu observations of wave direction and wave height both demonstrated good agreement with SWAN-predicted wave direction and wave height. Overall SWAN-predictions demonstrate good agreement with observations from both radar and insitu measurements.

Wave Propagation Processes at the Mouth of the Columbia River

by

Lisa Andes

A THESIS

submitted to

Oregon State University

in partial fulfillment of
the requirements for the
degree of

Master of Ocean Engineering

Presented June 19, 2007

Commencement June 2008

Master of Ocean Engineering thesis of Lisa Andes

presented on June 19, 2007

APPROVED:

Major Professor, representing Ocean Engineering

Head of the Department of Civil, Construction and Environmental Engineering

---

Dean of the Graduate School

I understand that my thesis will become part of the permanent collection of the Oregon State University libraries. My signature below authorizes release of my thesis to any reader upon request

---

Lisa Andes, Author

ACKNOWLEDGEMENTS

I would like to thank Dr. H. Tuba Özkan-Haller for her continued support, help, guidance, and patience throughout this project. I would also like to thank Dr. Harry Yeh, Dr. Merrick Haller and Dr. John Baham for serving on my committee. I would also like to thank Patricio Catalan and Merrick Haller for provided necessary data for my research. I would also like to thank John Stanely for constantly providing technical support. Lastly, I would like to thank my friends and family for their support. I feel very fortunate to have had the opportunity to interact with all of you.

TABLE OF CONTENTS

TABLE OF CONTENTS (Continued)

LIST OF FIGURES

LIST OF TABLES

1. INTRODUCTION

1.1 Introduction

The Columbia River serves as the border between Washington and Oregon, and is a widely used navigational inlet. The inlet is traversed by 12,000 commercial and 100,000 recreational vessels annually. These vessels export 14 billion dollars of goods from the Northwest each year to the global economy. The river is also home to one of the largest Dungeness crab markets in the United States; bringing 20 million dollars to the local economy annually, which does not include all of the other local commercial fisheries in the area (Moritz, 2007). However, the MCR has developed a longstanding reputation of dangerous navigational conditions. This reputation began when the first ship, the Columbia, traversed through the inlet in 1792. Today, over 2000 ships have sunk in or around the inlet (Wilma, 2006). The U.S. Coast Guard is also very active at the inlet. For example, in 1982 850 rescues were made at the Mouth of the Columbia River (MCR) and 10 lives were tragically lost (Gonzalez, 1984).

Hazardous conditions frequently occur when long period swell encounters ebb tidal currents over the Columbia River Bar (CRB), where wave breaking is most likely to occur. The CRB is located seaward of the inlet and spans the tips of the north and south jetties (Enfield, 1974) (Figure 1.1). However, rough conditions can persist from buoy 2–10 (Figure 1.1). The dangerous conditions that exist at the MCR cultivate a need to understand the dynamics of the environment. In this region winter storm waves can range from 4–10 meters with periods ranging from 12–22 seconds. Summer storm wave heights range from 2–4 meters with 7–12 second periods (Moritz, 2007). Ebb tidal currents often reach speeds of 2 m/s, which can result in a wave energy increase of up

to 50% from mid to low tide. (Gonzales, 1984).

Columbia River bar pilots close the bar for vessel passage when hazardous conditions exist over the bar. Bar Pilots serve as navigators for large commercial vessels (30–300 meters) traveling through the inlet. Currently, bar pilots rely heavily on intuition to make decisions on the navigability of MCR, arguing that provided forecasts are very conservative and cater to fishing vessels. Allowing passage into the inlet is critical to the commerce in the northwest. The conditions that the bar pilots are facing are shown in Figure 1.2. Forecasts lack the detailed information necessary to accurately make decisions about holding ships in Portland 6-8 hours before the vessel will be at the bar. Exploring techniques to provide real time data and accurate short term forecasts of this area would be advantageous to bar pilots when making decisions about bar closures.

The energetic wave conditions and strong currents prevalent to the area provide hazardous conditions for vessel passage as well as motivate sediment transport and threaten coastal infrastructure. This dynamic environment has been the site of many studies. For example, Michalson et. al. (2006) investigated the influence of borrow pits on the wave field on Peacock Spit. Existing wave heights are increased due to significant refraction on the spit. Waves curve around the north jetty, resulting in wave crests propagating perpendicular to the jetty. The analysis showed a burrow pit in the region could increase wave height on the order of 50%. Ruggerio et. al. (1997) investigated the extreme wave climate in the Columbia River littoral cell. The analysis estimated a 50 year wave height to range from 8.5 to 12 2 meters. This analysis was used to evaluate wave induced erosion in the littoral cell (Ruggerio, 1997). Gonzalez (1984) investigated the influence of wave-current interaction at the MCR. His work is discussed in Chapter 3. The MCR has also been the site of many sediment transport studies.

The purpose of this study is to evaluate the importance of wave-current interaction

at the MCR with a two dimensional model wave propagation model, SWAN (Simulating WAves Neashore) (Booij, 1999). SWAN is a spectral wave model that has been widely used in coastal areas, such as the MCR. For example, wave conditions were recently modeled in the California Bight by SWAN (Rogers, 2007) as well as the Chesapeake Bay (Lin, 2001).

SWAN simulations are also compared to remote sensing observations, a unique new technology that could provide real time conditions to bar pilots navigating through the inlet. Likewise, SWAN-computed wave height and and direction is compared to in-situ observations to validate SWAN computations at the MCR.

1.2 Site Description

The Columbia River is the second largest discharging rivers in the United States (Zhang, 2004). Summer and fall discharges range from 2800–11000 m^3/s during regulated flow periods. During peak ebb and flood tide conditions, discharge can reach an instantaneous flow rate of 51000 m^3/s and 28000 m^3/s, respectively (Moritz, 2007).

The channel is maintained by two jetties, north and south, constructed from 1885-1917. The jetties house the 3.3 kilometer entrance to the MCR. Two shoals have formed after jetty construction was completed and now serve as stability for the jetties. The first shoal is called Peacock Spit (Figure 1.1). This shoal is adjacent to the north jetty on the exterior of the inlet. The second shoal is located on the interior of the inlet adjacent to the south jetty, referred to as Clatsop Spit.

The dredged navigational channel is 8 km long, 905 m wide and 17 m deep and is maintained through regular dredging. Dredging removes 2.3–3.8 million cubic meters of sediment, annually. The sediment is deposited offshore at three locations. Currently, 65% of the dredged material is deposited seaward of the north jetty at the shallow water site, 10% goes to the North Jetty Site and the remaining 25% is deposited at a deep

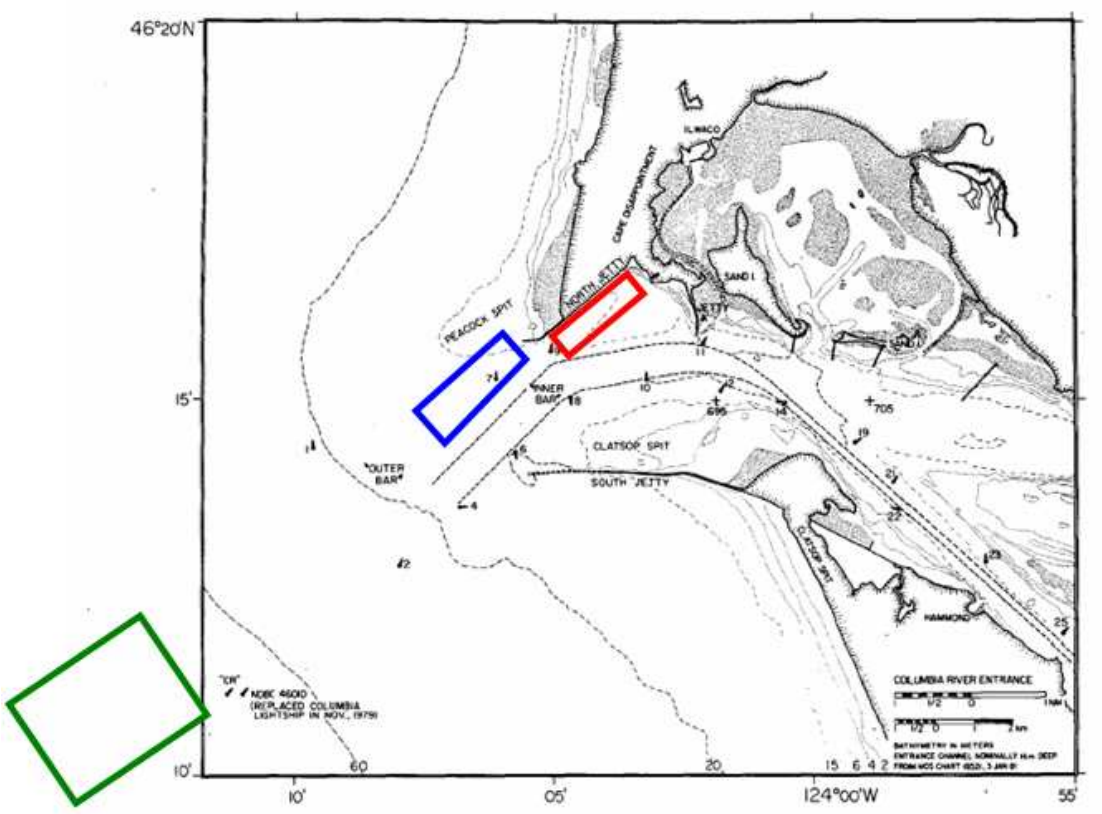

Fig. 1.1: MCR field site. Indicates the deep water disposal site (green) outside if the image, the north jetty site (red) and the shallow water site (blue). The navigational inlet is bound by the dashed lines in the mouth. The numbered points are US Coast Guard navigational buoys. (modified Gonzales, 1984)

Fig. 1.2: Wave conditions at the Columbia River Bar. Picture taken by a Columbia River bar pilot navigating a vessel through the channel (photo provided by R. Johnson, Columbia River Bar Pilots; 2007)

water disposal site (Figure 1.1).

A wave rider buoy (NDBC buoy 46029) is located three kilometers to the northwest of the southwest corner of the model domain (Figure 2.1), or 55 kilometers southwest of Astoria, OR. This buoy was used for all wave spectral information. The tide gage is located in Astoria (tide station 9440575), 17 kilometers inland of the MCR.

2. MODEL DESCRIPTION

2.1 Previous Work

The application of spectral wave models to coastal regions was developed in the 1990's. These models provide wave field predictions which can be used to aid in the understanding of coastal protection, environmental control and management. Additionally, these predictions can be a resource in the design of coastal structures including: ports, harbors, and navigational channels. One of these models is SWAN (Simulating Waves Nearshore) (Booij, 1999). SWAN is a third generation wave model that was especially developed for nearshore environments; as such, includes parameters for tidal currents and elevation changes.

Since SWAN's development, it has been widely used in many nearshore applications; however, only recent examples are discussed. Moghimi et. al. (2005) modeled wave conditions at the German Bight, located in the southeastern part of the North Sea, using SWAN. SWAN simulated the effects of current and tidal elevation changes on the wave field. In this region the tidal elevation change is $\pm$ 1.5 m and tidal current velocities reach speeds of 1.5 m/s. Wind was also used as an input parameter. Wave-wave interactions were accounted for in predictions of the wave field. Simulations were completed with and without the addition of current and tidal elevation input. The study concluded that the wave field was heavily influenced by strong currents and large tidal elevation changes. Overall SWAN compared well with observations; although, SWAN underestimated mean absolute period and over predicted wave height (Moghimi, 2005).

Work et. al. (2004) also used SWAN to model the wave conditions at Folley Island, South Carolina. These simulations were completed as part of a study to determine the

nearshore impacts of dredged pits around the island. Wind, tidal elevation, current and were used as input to SWAN. Of particular interest in the SWAN simulations was the onset of breaking; as such, the breaking coefficient was tuned. SWAN compared well to field measurements of wave height. The analysis also showed SWAN predictions were heavily influenced by tidal elevation changes; however, currents minimally affected the wave field (Work, 2004).

Lin et. al. (2001) also used SWAN to model the wave field in Chesapeake Bay. These simulations were used to make model-data comparisons in an effort to find a predictive model to that could be used to forecast wind-waves in the bay. SWAN input parameters included wind and bottom friction. SWAN simulations also accounted for triad wave-wave interaction. The analysis showed SWAN over predicted wave height and under predicted peak period when compared to observations (Lin, 2001).

Rogers et. al. (2007) also used SWAN to model the wave field in the Southern California Bight. This analysis was completed to assess the effect of operating SWAN in a stationary mode as opposed to the non-stationary mode. Simulations completed in stationary mode assume that wave propagation occurs instantaneously across the model domain. The stationary assumption also indicates that the wave response to model input, such as wind and bottom friction, occurs instantaneously over model domain. The non-stationary mode in SWAN allows the wave field to vary with time. The analysis concluded that using stationary mode increases the root mean square error moderately when making model data comparisons (Rogers, 2007).

SWAN has been used in many other applications to quantify wave field characteristics. This quantification aids in coastal policy and design practices.

2.2 Model Theory

SWAN is governed by the wave action balance equation. This is a form of the energy equation that accounts for the effect of currents on the wave field.

$$\frac{\partial}{\partial t}N + \frac{\partial}{\partial x}c_x N + \frac{\partial}{\partial y}c_y N + \frac{\partial}{\partial \sigma}c_\sigma N + \frac{\partial}{\partial \theta}c_\theta N = \frac{S}{\sigma} \tag{2.1}$$

N(x,y,t,σ,θ) is the action density of a spectral component of relative frequency, σ, and θ, as a function of time and space. Here N is defined as $\frac{E}{\sigma}$, where E is the energy density and σ is the relative frequency. For our purposes SWAN was utilized in stationary mode, hence $\frac{\partial N}{\partial t} = 0$. The second and third terms represent the advection of action density in geographic space with group speeds c_x and c_y. The fourth term represents the shift in the relative frequency (σ) resulting from changes in depth and currents with speed c_σ. The relative frequency, $\sigma = \omega - k \cdot U$, is representative of frequency measured by an observer moving with the current velocity, or a moving reference frame. The absolute frequency (ω), on the other hand, uses a fixed reference frame. Gradients in depth and current induced refraction with speed c_θ are represented in the fifth term. Generation/dissipation of energy density is symbolized by the sixth term (Booij, 1999).

SWAN solves Equation 2.1 by using a forward stepping implicit scheme; as such, the wave conditions at a grid point within the model domain are computed by the wave conditions of the surrounding grid points in x and y space. The scheme was developed for ambient depth uniform currents, using linear phase averaged equations (Booij, 1999). SWAN incorporates diffraction with a decoupled refraction-diffraction approximation (Holthuijsen, 2003).

2.2.1 Generation/Dissipation Mechanisms

The wave action generation within the domain is due to wind and triad and quadruplet wave-wave interaction. Quadruplet wave-wave interactions aid in the evolution of the wave spectrum in deep water by reassigning wave energy from the spectral peak to both higher and lower frequencies. The energy transferred to lower frequencies results in a repositioning of the spectral peak to a lower frequency. The energy transferred to higher frequencies is dissipated by whitecapping. Triad wave-wave interaction occurs in shallow water. Triad wave-wave interaction transfers energy from the spectral peak to higher frequencies that result in higher harmonics (Booij, 1999). Wind input is excluded in our analysis. Additionally, our model simulations will not be accounting for wave-wave interactions. These terms are excluded in our analysis because the domain is small, implying that we are specifically investigating remotely generated swell.

Wave action dissipation is accounted for with whitecapping, bottom friction and depth-induced breaking. Only depth induced breaking will be considered, although we will discuss the effects of whitecapping in Chapter 4. SWAN uses the Battjes and Jansen (1978) depth-limited random wave breaking model. It includes a variable breaking coefficient, γ (Nelson 1987, 1994), that is dependent on bottom slope, using

$$\gamma = 0.55 + e^{-0.012 \cot \beta} \tag{2.2}$$

where β is a bottom slope. This relationship is used for β greater than 0.01, otherwise a γ of 0.73 is used. The computed γ is used as input to the depth-limited random wave breaking model to compute the maximum wave height of the broken wave.

2.3 Model Input

SWAN requires two main types input: bathymetry and wave spectral information at the boundaries. Additional information can be specified if available, including current, tidal elevation, wind and bottom friction coefficient. Bottom friction and wind are not likely to be the dominant physics here because the model domain is small, and are not specified in our analysis. The model domain is defined in Section 2.3.2.

2.3.1 Wave Spectra

Offshore spectral information is obtained from an offshore buoy (NDBC 46029 / 46.14 N 124.51 W). The raw spectral information is obtained in the form of coefficients R_1, R_2, α_1 and α_2. These coefficients, in concert, produce a spectrum using

$$S(f,\theta) = C_{11}\frac{1}{\pi}(0.5 + R_1\cos(\theta - \alpha_1) + R_2\cos(2(\theta - \alpha_2))) \tag{2.3}$$

where θ is the direction bins ranging from 182.5 to 357.5^o true north. C_{11} is the spectral density provided by the buoy over the frequency range of 0.02 to 0.485 Hz. The spectral information was converted to the model domain where 0^o is normally incident, +90^o is waves traveling to the north, and -90^o is waves traveling to the south. This spectral information was entered on each side of the domain with the exception of the shoreline (north, south, and west sides). Thus the spectral information is assumed to be constant along the boundaries of the domain.

The model bathymetry was provided by A. Baptista (used for CORIE-group simulations, OHSU), and was constructed using USACE bathymetry from winter and spring surveys of 2003 and 2004, respectively. In the nearshore zones bathymetric surveys provided by Ruggerio (2005) were inserted into the domain. The nearshore surveys covered the regions north of the north jetty (Benson Beach) and south of the south jetty.

2.3.2 Model Domain

The domain has sand bar systems, shoals (Peacock and Clatsop Spit), dredge deposit mounds, a dredged navigational inlet, an offshore canyon, and north and south jetties framing the inlet (Figure 2.1). The offshore canyon is the deepest part of the model domain at 520 m. The model domain was 39.7 km in the cross-shore and 36.7 km in the alongshore direction centered on the MCR. The grid resolution was 50X50 meters.

Additional SWAN simulations were carried out for time periods when the buoy was located closer to shore (46.18 N and 124.19 W). As a result the domain in the cross-shore direction was reduced to 17.8 km, which is represented by the green line in Figure 2.1. For these cases the domain resolution was increased to 20X50 meters in the cross shore and along shore directions, respectively.

2.3.3 Current and Tidal Water Level Input

For the purposes our analysis depth uniform ambient currents and tidal elevation fields were used as input to SWAN. SWAN calculates wave-current interaction with provided currents. Only tidal currents were considered in our analysis. Thus, wave-induced current fields were not included. Both currents and tidal elevations were calculated by CORIE (A. Babtista). The tide gage in Astoria (tide station 9440575) was also utilized when CORIE data was unavailable.

The model domain used to compute the current and tidal elevation covered the majority of the west coast of the United States and parts of Canada. The southern boundary of the domain is Southern California. The northward part of the domain is British Columbia. The eastward boundary is 240 km beyond the inlet entrance. The westward boundary of the domain extended west of the continental shelf of California (Baptista, 2005).

The model forcing included river, oceanic and atmospheric conditions. River forcing

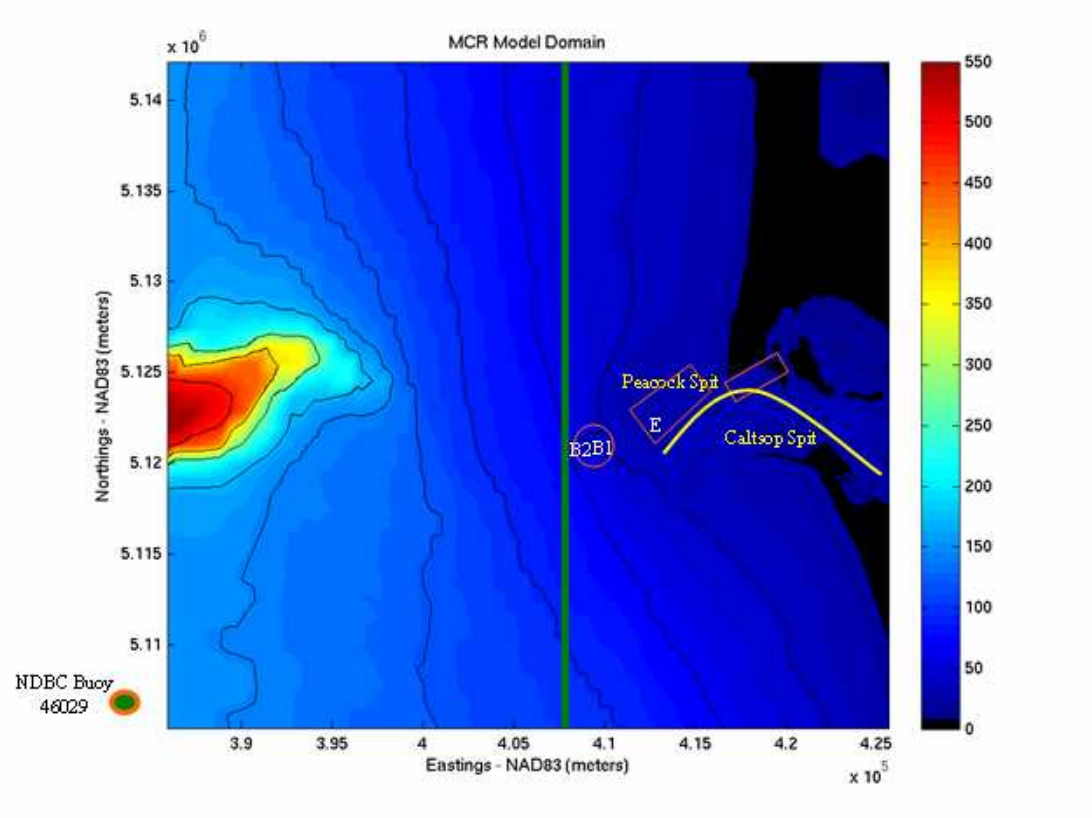

Fig. 2.1: MCR Model Domain. The color bar represents water depth. Green line represents the size of the new domain when the buoy location was moved shoreward. The white labels represent locations where insitu observations were made. From left to right: B2, B1, and E. The offshore canyon is on the far left-center of the domain. The yellow line in the inlet indicates the dredged navigation channel. The yellow labels indicate Clatsop Spit to the south and Peacock Spit to the north. The rust colored shapes indicate offshore dredge disposal sites.

input is river discharge. Oceanic forcing input is tidal constituents, tidal amplitudes, tidal phases, salinity and temperature. Atmospheric forcing is wind, surface atmospheric pressure, and air temperature (Baptista, 2005). The forcing was used to compute depth averaged currents and tidal elevation at the mouth of the inlet. Current and tidal elevation changes computed by CORIE are validated inside the estuary by numerous observations; however, the model input has not been validated outside of the estuary.

3. WAVE-CURRENT INTERACTION AT THE MCR

3.1 Previous Work

As large wave interact with strong currents, waves can steepen and even break which can be a tremendous navigational hazard. The rough conditions can even lead to vessel capsizing (Chawla, 2002). Hazards resulting from wave-current interaction can occur at inlets. Each inlet has responds uniquely to wave-current interaction. For example, Smith et. al. (2001) investigated the Ponce de Leon Inlet in Florida to evaluate the importance of wave-current interaction. The Ponce de Leon Inlet has maximum tidal currents of 1 m/s and a tidal range of 1 m. Smith completed his analysis using STWAVE (steady-state spectral WAVE model) (Resio, 1987) to conduct simulations including and neglect tidal current. STWAVE is spectral wave model, similar to stationary mode of SWAN. Model input was wave spectral information at the domain boundary, as well as current and tidal elevation fields. The analysis indicated that the root mean square difference between the including and neglecting current cases indicated a maximum change in wave height of 3.7% and 2^o shift in wave direction. As a result of the analysis, it was concluded that the wave field was minimally influenced by currents at Ponce de Leon inlet (Smith, 2001).

Osuna et. al. (2004) also investigated the importance of wave-current interaction in the Southern North Sea (SNS). Maximum tidal currents at the SNS are under 1.3 m/s and maximum tidal elevation at the SNS is 4.5 m. The purpose of this study was to predict the impact of storm events on coastal infrastructure. As a result, the tidal elevation values include storm surge. Wave-current interaction was modeled by WAM *Cycle 4*. WAM is a third generation wave model, also similar to SWAN. The model

input included spectral information at the domain offshore boundaries, as well as wind, current, tidal elevation input fields. The analysis concluded that the increase in wave height resulting from the addition of currents exceeded 5%. The influence of current on the wave field was least significant in deeper regions of the SNS (Osuna, 2004).

Work et. al. (1997) also investigated the importance of wave-current interaction at Pensacola Pass, Florida. The study was conducted to evaluate the influence of wave-current interaction on nearby shoals of the inlet. Mean currents reached velocities of 0.34 m/s. The model used to compute the importance of current on the wave field was REF/DIF1. REF/DIF1 computes wave fields using a parabolic assumption for the mild slope equation and accounts for both wave refraction and diffraction in its simulations. The analysis indicated a 6% increase in wave height resulting from the addition of current in the model simulations. In this study it was concluded that currents had little effect on the wave field at the observation location which was located over 1 km away from the inlet mouth. Wave-current interaction effects are observed by vessels traversing through the inlet, which suggested observations should be located closer to the mouth for further investigation (Work, 1997).

Gonzalez (1983) also investigated wave-current interaction at the Mouth of the Columbia River (MCR). The MCR frequently has tidal currents that exceed 2 m/s. To model the effect of wave-current interaction at the inlet a one-dimensional model that accounted for refraction and shoaling was used. The model domain was defined as a transect along the main axis as the navigational channel. The one dimensional model assumes the contours are uniform perpendicular to the transect. Assuming uniform contours perpendicular to the transect implies that influence of refraction or focusing due to bathymetric features or currents is not considered in the analysis. The analysis considered swell and wind waves independently. Swell wave heights were under estimated on ebb tide. Wind wave heights were also underestimated on ebb tide and over

estimated on flood tide. The errors in prediction of wave height for both wind and swell waves were thought to be due to two dimensional shoaling and refraction effects. Wave-current interaction at the MCR is reevaluated, in this study, to investigate the effects to investigate the influence of current on the wave field (specifically wave height, length and relative period) with SWAN.

3.2 Wave-Current Interaction Theory

The effect of current on the wave field is demonstrated by the relationship $\sigma = \omega - k \cdot U = \sqrt{gk \tanh(kh)}$, where σ is the relative frequency, ω is the absolute frequency, k is the wave number, U is the current velocity and g is gravitational acceleration. If we apply this relationship to a case where currents oppose wave propagation, σ and k will both increase with an increasing current strength. The increase in σ and k indicates a decrease in relative period (T_r) and wave length (L). However when currents follow the direction of wave propagation the inverse is true, σ and k decrease, indicating and increase in L and T_r. If the direction of current in perpendicular (90^o) to the direction of wave propagation the current does no influence on the wave field.

The influence of a current on wave height (H), is related to group velocity (C_{ga}). Here $C_{ga} = \frac{\partial \omega}{\partial k} = C_{gr} + U \cos \mu$, where μ is the angle between the U and the k vector. This relationship indicates that when currents oppose wave propagation ($\mu = 180^o$), C_{gr} decreases. The inverse is true when currents follow ($\mu = 0^o$) the direction of wave propagation. Energy flux is conserved prior to wave breaking, $EC_{ga} = E(C_{gr} + U \cos \mu) = constant$, holds true, where $E = \frac{1}{8} \rho g H^2$. This relationship indicates that when C_{ga} decreases, such as in the case of opposing currents, H increases. Likewise, in the case where C_{ga} increases, in a case of following currents, H decreases. Wave blocking/breaking will occur if $C_{ga} = U \cos \mu$.

At inlets, opposing and following currents are often tidally dominated (Svendsen,

2005). As a result, wave-current interaction is a concern at many inlets. It is of interest to identify the influence of currents and tidal elevation on wave characteristics at the MCR. The MCR has a semi-diurnal tidal cycle, with a tidal range of 2.6 meters, and tidal currents approach 2 m/s.

To evaluate the importance of wave-current interaction, SWAN model simulations were completed for the dates of January 16-19, 2006. Wave conditions recorded by the buoy are shown in Figure 3.1. Wave heights range from 3–7 meters. Waves are going towards the north and east. Mean periods ranged from 7–12 seconds.

SWAN was utilized, first considering wave-current interaction by applying a tidal current field over the model domain and second neglecting tidal currents. Both simulations included tidal elevation fields as model input. The tidal datum used was NGDV29. Model simulations were dependent on times when current information was provided. Current and tidal elevations were provided every three hours, from January 16, 2006 at 01:00 to January 19, 2006 at 22:00 hours; as such, eight runs per day (32 total runs) were completed for both cases during the time series.

Ebb tide currents will be referred to as opposing currents, indicating that ebb currents oppose the direction of wave propagation. Flood tide currents will be referred to as following currents, denoting that flood currents follow the direction of wave propagation. This convention will also be used in this and subsequent sections. Additionally, current values will be reported in the magnitude of the u (cross-shore) and v (alongshore) components. The magnitude of the current will have the sign of the u term since we are particularly interested in when the current is coming in (+) or going out (-) of the mouth of the inlet.

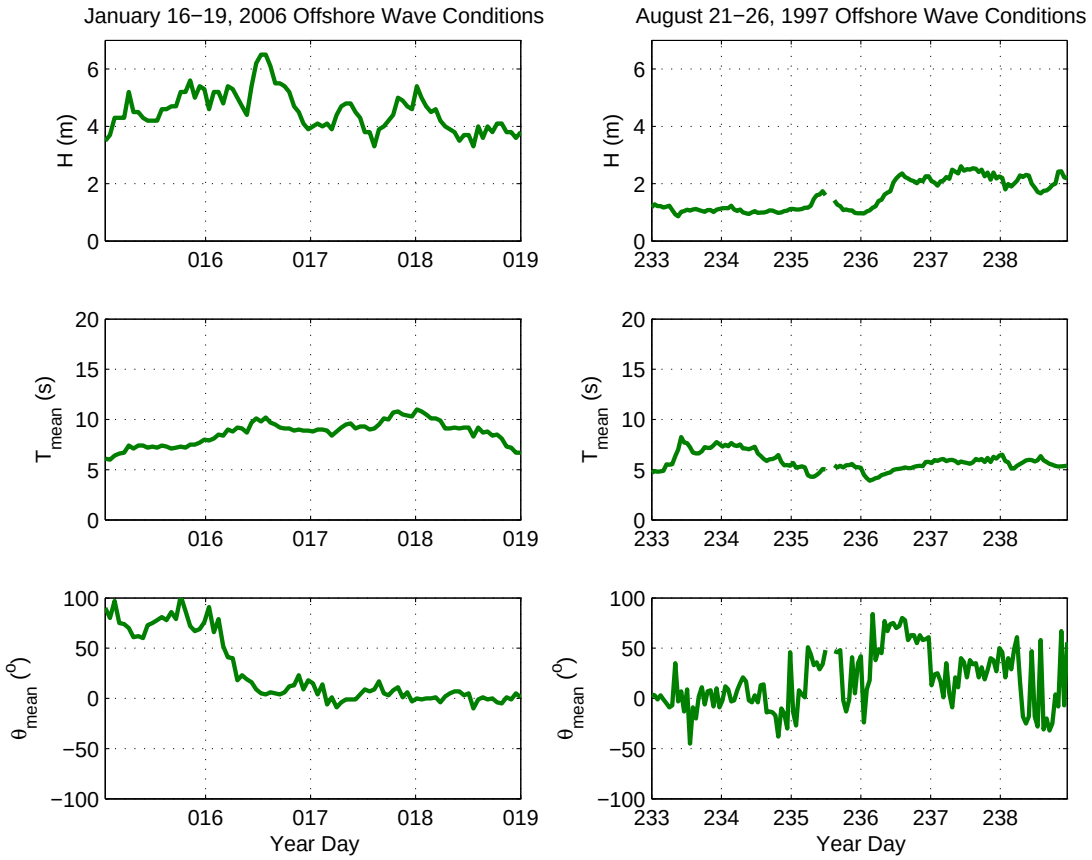

Fig. 3.1: Wave conditions (H, T and θ) from buoy 46029 from January 16–19, 2006 (left) and August 21–26, 1997. The θ is shown as the direction where the waves are going to.

3.3 Results

Two examples were chosen to show a qualitative assessment of the model simulations, an opposing current case and a following current case. The examples are shown in Figures 3.2, 3.3 and 3.4. Figure 3.2 (Top) represents an opposing current case neglecting wave-current interaction. In this figure the wave height at the offshore boundaries is 3.7 m. The wave height increases at a dredged deposited mound seaward of the inlet and over Peacock Spit. Wave height also decreases with the onset of breaking close to shore. When current is added to this simulation, Figure 3.2 (Bottom), the same wave height is observed at the offshore boundaries, as well as over Peacock Spit; however, there is a very defined increase wave height concentrated at the inlet that can be visually observed.

The same analysis is completed for the following current example (Figure 3.3). Figure 3.3 (Top) is the simulation neglecting currents. Here the offshore wave height is also 3.7 m and wave height increases over the dredged mound as well as Peacock Spit. When current is included in the simulation a decrease in wave height centered at the inlet can be observed (Figure 3.3 (Bottom)). However, the decrease in wave height is not as pronounced as the increase in wave height shown in the opposing current case.

We were interested in quantifying the change in wave conditions resulting from wave-current interaction in the model simulations. To quantify the wave field, the change in H, L and T_r were calculated. Figure 3.4 represents the ΔH for the opposing and following current examples previously evaluated qualitatively. Here ΔH was calculated by subtracting the wave height values of the neglecting current simulations from values computed from the including current simulations ($\Delta H = H_{current} - H_{nocurrent}$). The change in wave height in the opposing current case (Figure 3.4 (Top)) shows an increase in wave height concentrated at the mouth of the river that exceeds 1 m. In the following current case (Figure 3.4 (Bottom)), a decrease in wave height is observed on the order

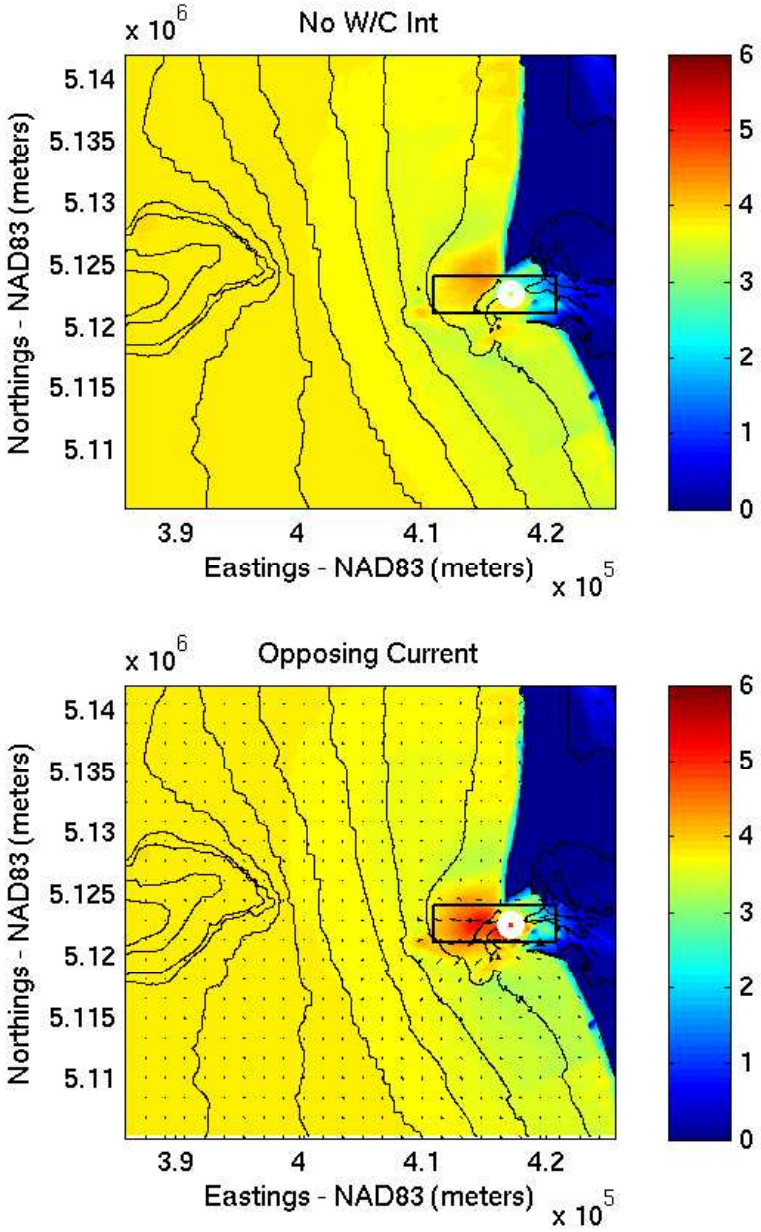

Fig. 3.2: These figures represent Year Day 19 at 19:00, an opposing current case. Top–Wave height neglecting wave-current interaction. Bottom–Wave height including wave current interaction as an input parameter. The arrows in the figure indicate the current direction. The black box defines a control area used to make further comparisons. The white circle in the center of the box is the location of wave-current interaction at a point location.

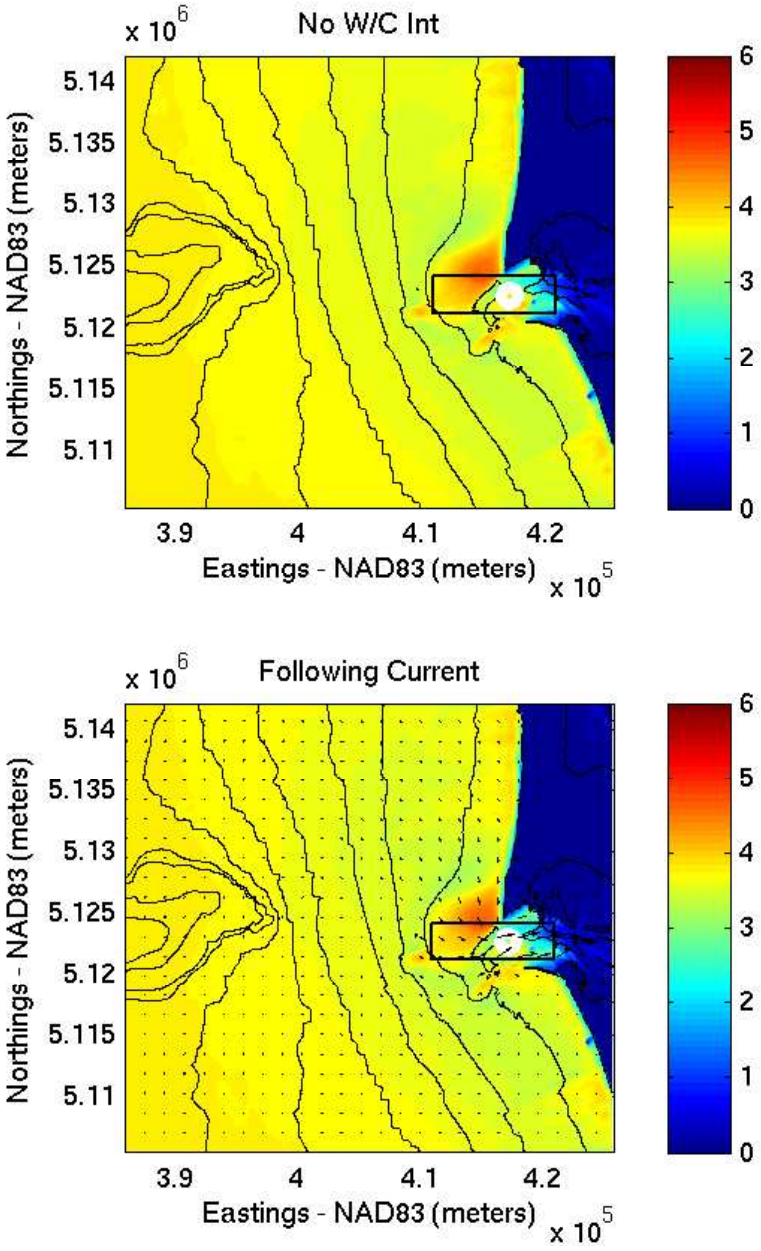

Fig. 3.3: Year Date 18 at 01:00, a following current case. Top–Wave height neglecting wave-current interaction. Bottom–Wave height including wave current interaction as an input parameter. The arrows in the figure indicate the current direction. The black box defines a control area used to make further comparisons. The black star in the center of the box is the location of wave-current interaction at a point location.

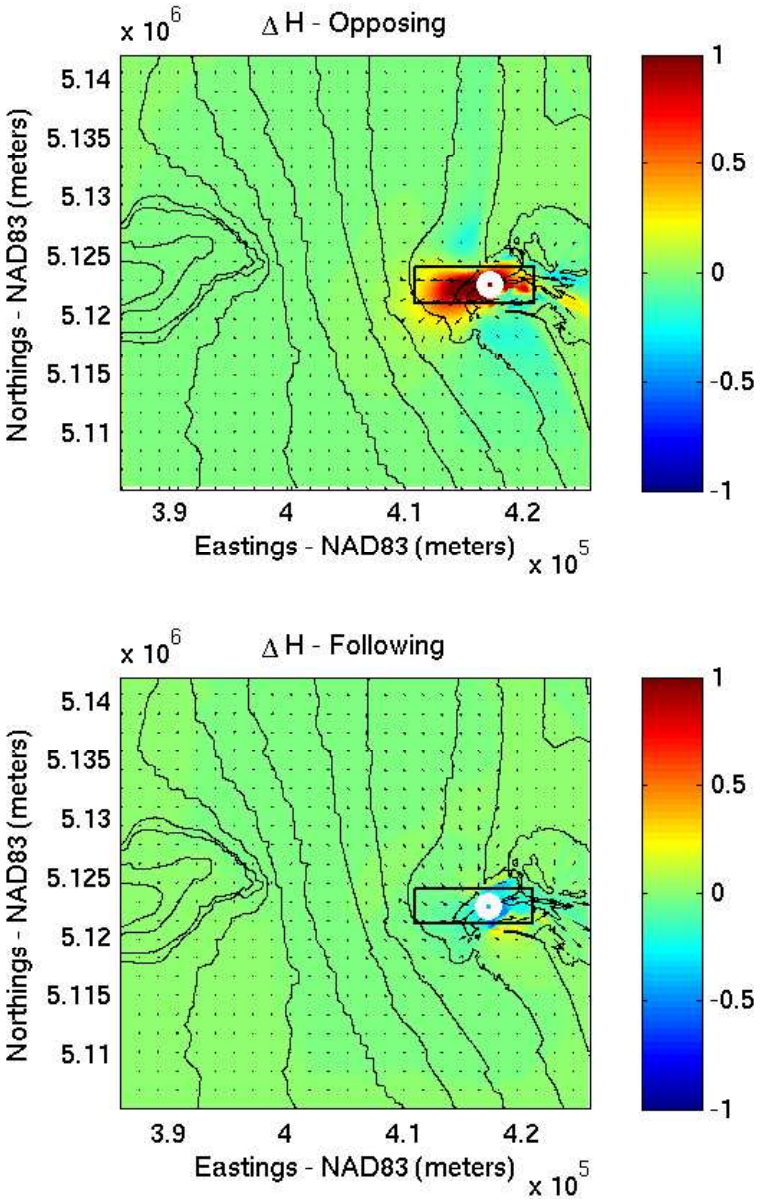

Fig. 3.4: These figures represent ΔH for an opposing and following current cases. The opposing current case is year day 19 at 19:00, and the following current case is year day 18 at 01:00. The boxed area is used to make further comparisons. The black star in the center of the box is the location of wave-current interaction at a point location.

of 0.5 meters. The reduction in wave height is also concentrated at the inlet; however, visually the decrease in wave height is not as defined as the increase in wave height from the opposing current case.

The change in wave characteristics (ΔH, ΔL, and ΔT_r) will be computed by subtracting the simulations neglecting current from the simulations including current, and will be evaluated in two ways. First, a point was chosen at the center of the MCR (Figures 3.2, 3.3 and 3.4 Easting=417149.02, Northing=5122640.60) to track the changes in wave characteristics over the study period (Figure 3.5). The point location is identified by the white circle in Figures 3.2, 3.3 and 3.4. At this location, opposing currents (-) exceed 1 m/s with a maximum current of 1.66 m/s (Table 3.1). Following currents (+) only exceed 1 m/s twice during the study period, with a maximum current of 1.25 m/s (Table 3.1). The currents oscillate from opposing to following currents with a semi-diurnal tide cycle. The changes in H, L, and T_r reflect the same semi-diurnal tidal signature shown in $U_{magnitude}$ and η in Figure 3.5.

The mean and maximum changes in wave conditions at the point location for both following and opposing tidal currents are shown in Table 3.1. Tidal currents reached peak following current values at 01:00 and 13:00 hours each day during the study period. The change in H, L, and T_r resulting from following tidal currents were averaged at these times to find the mean value (Table 3.1). The maximum change in these wave characteristics at this location are also recorded in Table 3.1. Tidal currents reached peak opposing current values at 07:00 and 19:00 hours of each day (offset by six hours from the incoming tide, characteristic of a semi-diurnal system). Likewise, the change in H, L, and T_r resulting from opposing tidal currents were averaged at these times to find the mean value (Table 3.1).

From this analysis, H increased while L and T_r decreased with opposing currents. The opposite is true during following current cases, H decreased while L and T_r in-

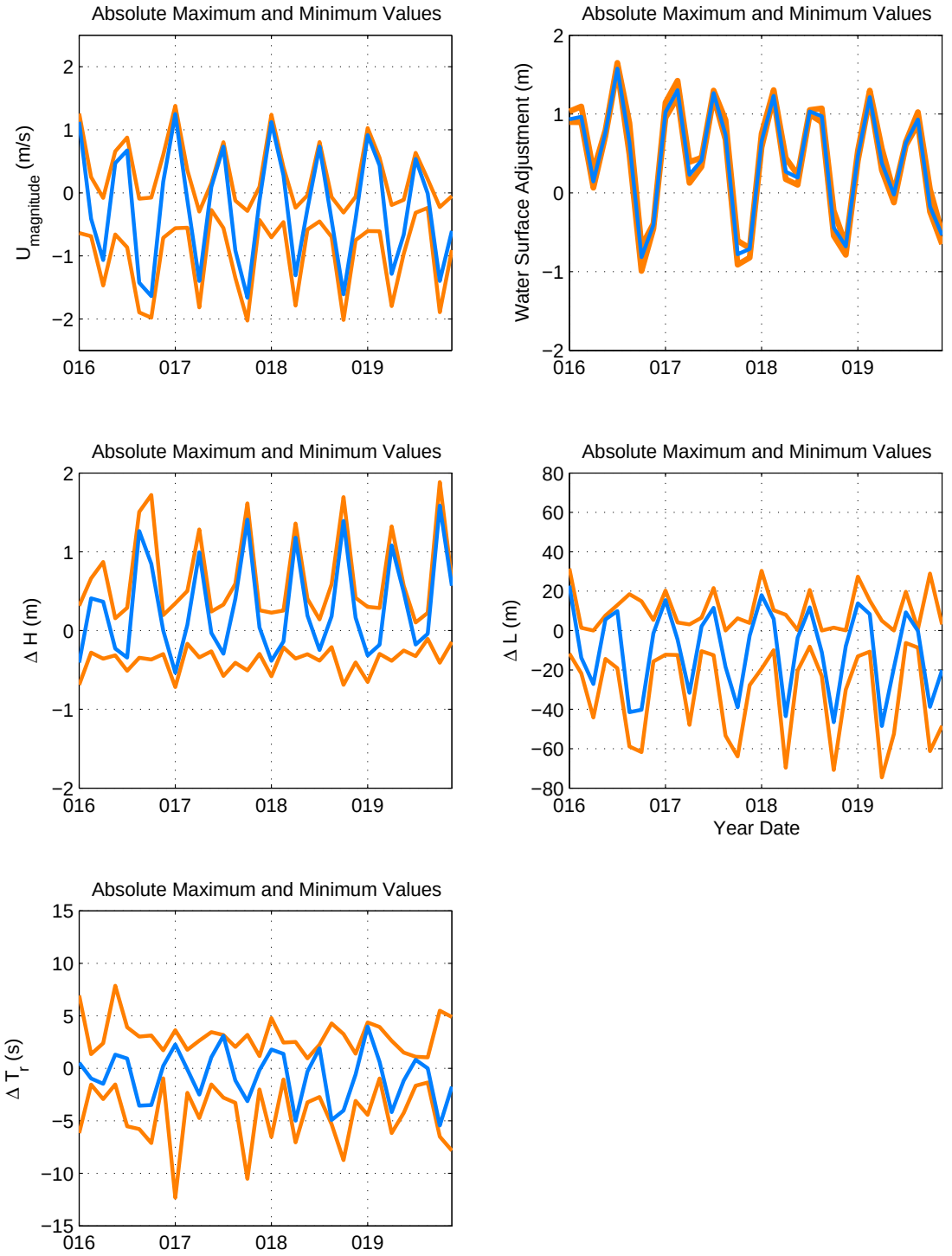

Fig. 3.5: Top Left: At point Easting=417149.02, Northing=5122640.60 change in wave characteristics (H, L, and T_r), tidal currents U_{mag} and tidal water surface adjustment (blue). Absolute maximum and minimum (marigold) changes in ave characteristics (H, L, and T_r), tidal currents U_{mag} and tidal water surface adjustment within the outlined box in Figures 3.2, 3.3 and 3.4.

Table 3.1: Maximum and mean changes in wave height, length and relative period at Easting=417149.02, Northing=5122640.60.

	Opposing Currents		**Following Currents**	
	Mean	**Max**	**Mean**	**Max**
Δ Wave Height (m)	1.11	1.59	-0.34	-0.54
Δ Wave Length (m)	-39.40	-48.50	14.06	22.80
Δ Relative Peak Wave Period (s)	-5.45	-4.41	1.92	3.98
$U_{magnitude}$ (m/s)	-1.42	-1.66	0.89	1.25
Tidal Elevation (m)	-0.15	-0.82	0.95	1.58

creased. The magnitude of the changes in H, L and T_r are greater during opposing tide (Table 3.1).

Secondly, the maximum and minimum values of ΔH, ΔT_r, ΔL, $U_{magnitude}$, and η within the control area defined by the box in Figures 3.2, 3.3 and 3.4 were identified for every case in the time series. These values were calculated to identify an envelope of values that correspond to current induced changes in wave characteristics, currents and tidal elevations. The maximum and minimum change in wave characteristics did not occur at the same location within the control area for every case. The absolute maximum and minimum values are plotted in Figure 3.5. The same trend exists in the control are at the mouth of the inlet for ΔH, ΔT_r, and ΔL as well as $U_{magnitude}$ and η as at the point location. For example, wave height increases during opposing current periods and decreases during following current periods. The change in wave conditions found within the control area are used to compute an envelope (Table 3.2). The changes in wave conditions found within the control area were of greater magnitude then the point location.

When calculating the minimum values for ΔL and ΔT_r shown in Table 3.2 a sharp bathymetric gradient was discovered on the north side of Clatsop Spit. This gradient was located within the control area where the maximum and minimum values were found. The maximum and minimum values were used to define an envelope of the

Table 3.2: Absolute maximum, minimum and mean changes in wave height, wave length and period in boxed region.

	Opposing Currents		**Following Currents**	
	Mean	**Max**	**Mean**	**Max**
Δ Wave Height (m)	1.46	1.88	-0.55	-0.72
Δ Wave Length (m)	-61.76	-74.54	23.04	31.51
Δ Relative Peak Wave Period (s)	-6.72	-10.51	3.97	7.86
$U_{magnitude}$ (m/s)	-1.84	-2.03	1.00	1.38
Tidal Elevation (m)	-0.25	-0.99	1.01	1.65

change in wave conditions. This gradient resulted in unrealistic values of L and T_r in the wave-current interaction model output. As such, this region was neglected in the analysis of ΔL and ΔT_r predictions of the envelope.

3.4 Discussion

SWAN has demonstrated that wave-current interaction can have a significant effect on wave characteristics at the MCR. Maximum opposing and following current velocities reached 2.03 and 1.38 m/s, respectively. Opposing currents are 32 percent greater than following currents at the MCR during this study. Strong currents have a significant impact on wave characteristics. Opposing currents can have maximum increases in H of 1.88 meters and a maximum decreases in L of 74.54 meters. Following currents can have maximum decreases in H of 0.72 meters and maximum increases in L of 31.51 meters, indicating that ΔH and ΔL are 60.6 and 57.7 percent, respectively, larger during opposing current cycles. The results demonstrate opposing currents have the greatest effect on wave characteristics at the MCR; however, both opposing and following currents make a significant impact on wave characteristics. SWAN results including wave-current interaction will be compared to radar and in-situ observations in subsequent sections.

4. OBSERVATION-MODEL COMPARISONS

4.1 Comparison of Remote Sensing Data and Model

A Sitex marine X-band radar (RADARpc25.9) and data acquisition system was used to collect field measurements at the Mouth of the Columbia River (MCR) (Figure 4.1). The radar was deployed at the region just to the north of the MCR (Figure 4.2 Northing=5124872/Easting=417207). The deployment was from January 16-19, 2006 at a land based station. The study area is 5 kilometers radially (Figure 4.2). The radar range covers Peacock Spit, sand bars seaward of Benson Beach and the northern portion of the navigational channel. Fifteen minutes of data was collected at the beginning of every hour at the field site. From this data, wave direction and breaking information were extracted (Catalan, 2007).

4.1.1 Wave Direction

To make comparisons with SWAN of wave direction, the radar estimated wave angles are transferred onto a rectangular domain 2800 meter in the cross shore by 3200 meters in the along shore direction (Figure 4.2). From the field deployment 14 cases were selected for comparison. These correspond to times when current data was available and radar data sets were passed quality control. Wave direction characteristics were extracted with a discrete Fourier transform for frequencies: 0.067, 0.100 and 0.133 Hz, using a method described in Plant et. al., 2007. Frequency bands were chosen to capture the incident wave field ranging from 0.05-0.17 Hz. All results are shown for the frequency 0.067 Hz. This frequency corresponds most closely to the peak frequency reported by the buoy. To assess the quality of each observation, a skill value for the estimated wave

Fig. 4.1: Shore-based marine radar deployment. Antenna is mounted 4 meters above sea-level (Haller, 2007)

angles was determined at each point in the rectangular domain. The skill value was found by normalizing the estimated wave directions by the signal at the jetty where no wave information could be obtained (Catalan, 2007). Skill values range from 0 to 100%.

A sample case was chosen to represent all 14 model cases, year day 18 at 16:00 hours; however, a quantitative analysis of all 14 cases will be discussed in a subsequent section. This case is shown in Figure 4.3. The white areas in the figure are representative of regions where the radar skill was less than the chosen threshold value of 50. Wave directions of $+90^o$ represent wave propagation to the north.

Sample Case Comparison

Estimated wave directions from SWAN and radar show good agreement (Figure 4.3). In the northern part of the domain (Figure 4.3), SWAN indicates waves propagating shoreward normally incident and from mild angles both from the southwest and northwest. This is comparable to the wave directions shown by the radar (Figure 4.3). In

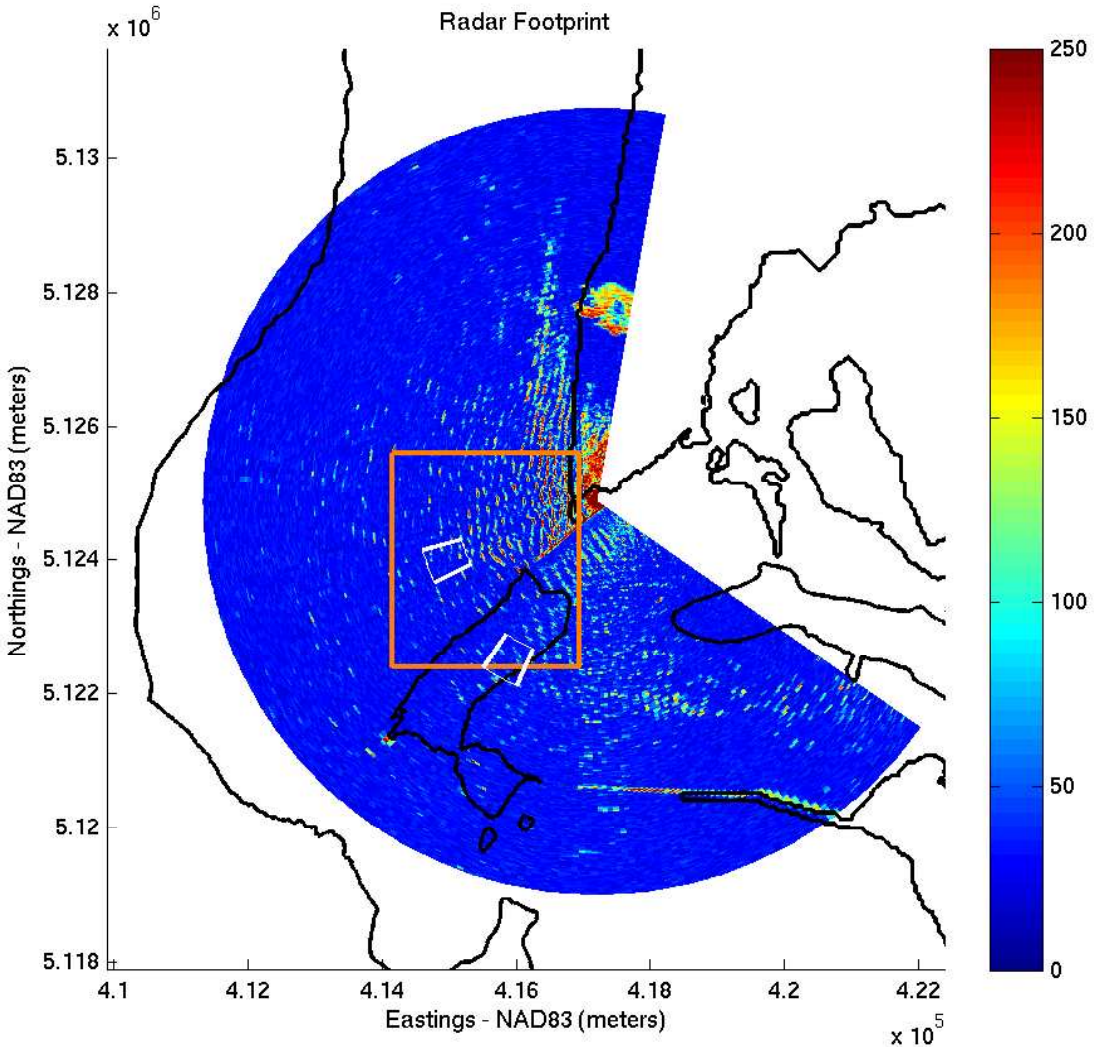

Fig. 4.2: MCR with radar model domain. White boxes are locations radar data was used to compare wave breaking with SWAN, Shoal (northern most box) and Channel (southern most box). The rust box is location used to compare wave direction with SWAN.

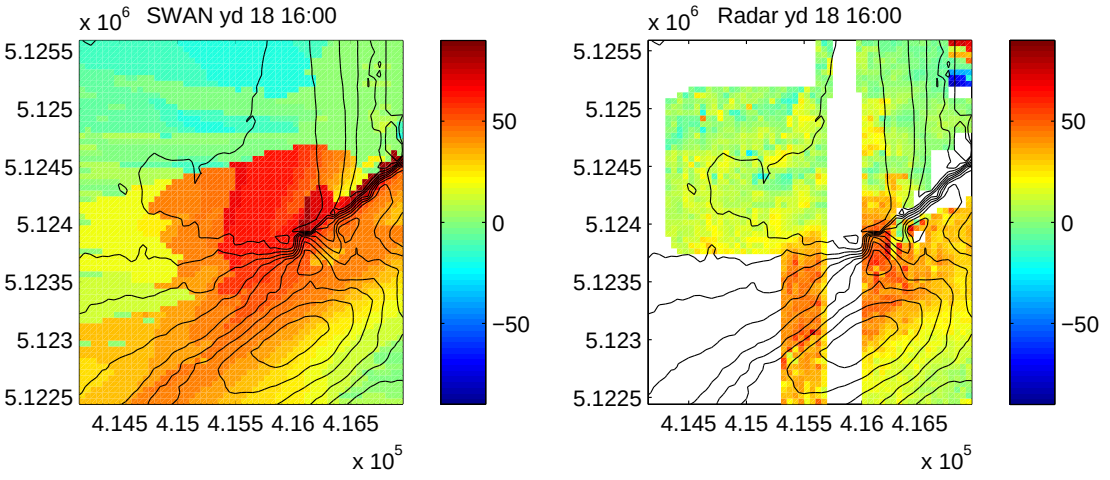

Fig. 4.3: Right: Marine Radar extracted qualitative wave direction for Year Date 18 at 16:00 results. **Left:** SWAN qualitative wave direction for Year Date 18 at 16:00 results.

the southern region of the figure SWAN predicts waves propagate shoreward obliquely to the north. This same pattern is observed in the radar image. However, the central part of the figure, just north of the jetty, there is less agreement in the radar and SWAN images. The north jetty is indicated by the converging diagonal contours beginning on the right side of Figure 4.3. SWAN estimates oblique propagation northward to shore while the radar estimates waves propagating normally incident in the same region. The disagreement in the images occurs at Peacock Spit.

Both the SWAN and radar images are plotted together in a quiver plot (Figure 4.4). The agreement is very good in the channel and in the northern part of Benson Beach, where the arrows corresponding to wave direction from both SWAN and radar are nearly aligned on top of each other. There is considerable disagreement in the area north of the north jetty. In this area the arrows are almost normal to each other.

An alongshore transect marked by the black line in Figure 4.4 was used to make quantitative comparisons. To smooth the radar-estimated angles a three point (150 meter) running average was computed and shown in Figure 4.4. These averaged values

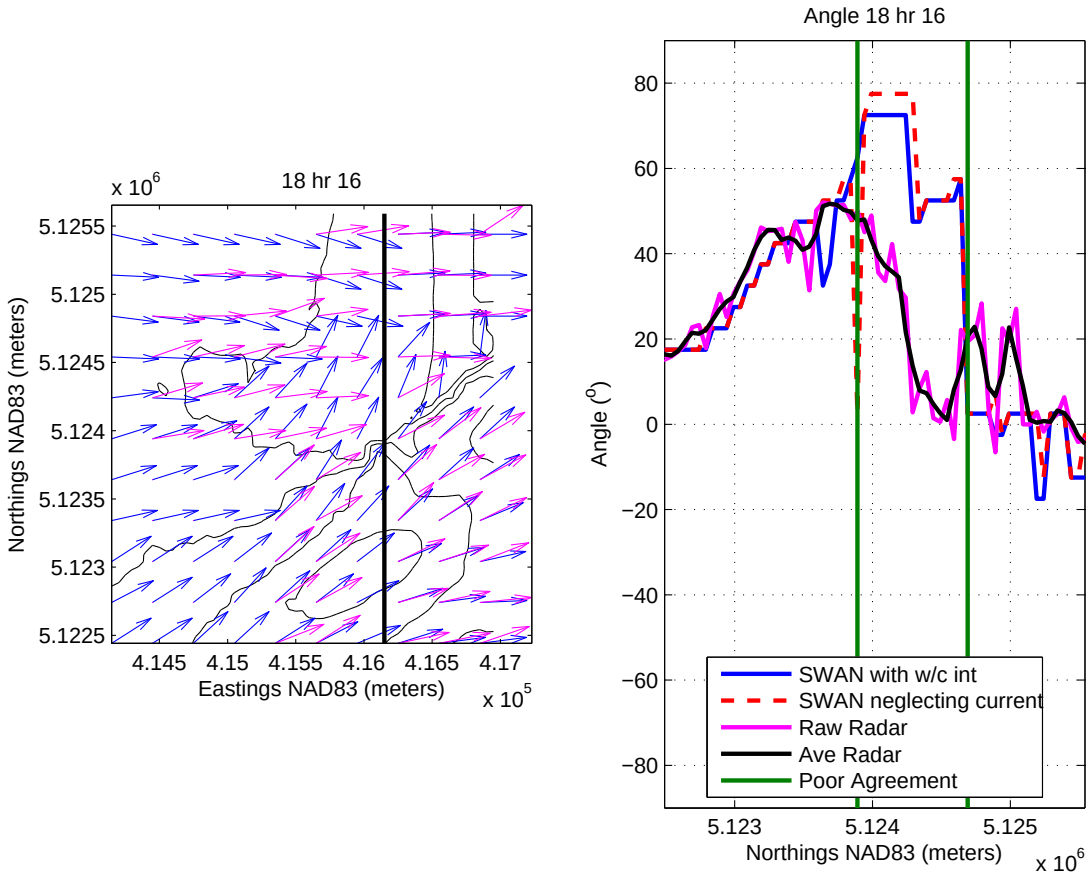

Fig. 4.4: **Left:** Quiver plot of SWAN wave directions (blue) and radar wave directions (magenta). **Right:** Transect outlined by the figure on the left of SWAN wave direction including the effects of wave-current interaction (blue), SWAN wave direction neglecting tidal currents (dashed red), raw radar calculated wave direction (magenta), radar calculated wave angles with a 150 meter running average (black). The vertical green lines are used to define the area of poor agreement in the center of the transect.

will be used to compute a regression analysis in the following section. The transect reflects the qualitative observations made in Figures 4.3 and 4.4, in particular, there is good agreement in the navigational channel (the left side of the transect) and at Benson Beach (the right side of the transect). In approximately the center of the transect, north of the north jetty, the strongest disagreement occurs (Northing 5.124e6–5.1245e6). In this region of the transect SWAN estimates the wave angle as (from left to right) 72.5^o degrees for 350 meters. Followed by a steep decrease in angle to 52.5^o that remains constant for 300 meters. The radar estimated angles, on the other hand, have a negative gradient and descend to zero degrees. The green lines shown in Figure 4.4 bound the region of disagreement. This region will be given special consideration when a regression analysis is completed on the data set in a subsequent section.

The root mean square error (RMSE) between SWAN (including current) and the radar-estimated wave directions was calculated. This is shown in Figure 4.5. The RMSE for each frequency band of the radar-estimated wave direction results was computed. These frequency bands are 0.067, 0.100 and 0.133 Hz. All frequency bands show the largest RMSE occurs in the region just north of the jetty, bound by the green vertical lines in Figure 4.5. The mean RMSE along the transect for each frequency value, excluding the area of disagreement, is 13.78, 15.04, and 16.58 degrees for frequency bands 0.067, 0.100 and 0.133, respectively. When the area of disagreement is included, the mean RMSE is 22.81, 23.41, and 24.85 degrees, respectively.

Results from Other Cases

A regression analysis was completed on the 14 comparisons made of radar-estimated and SWAN-predicted wave directions along the transect. The regression analysis compares SWAN (including currents) with the radar-averaged wave directions. The regression was first computed excluding the region of poor agreement outlined in Figure 4.4 with

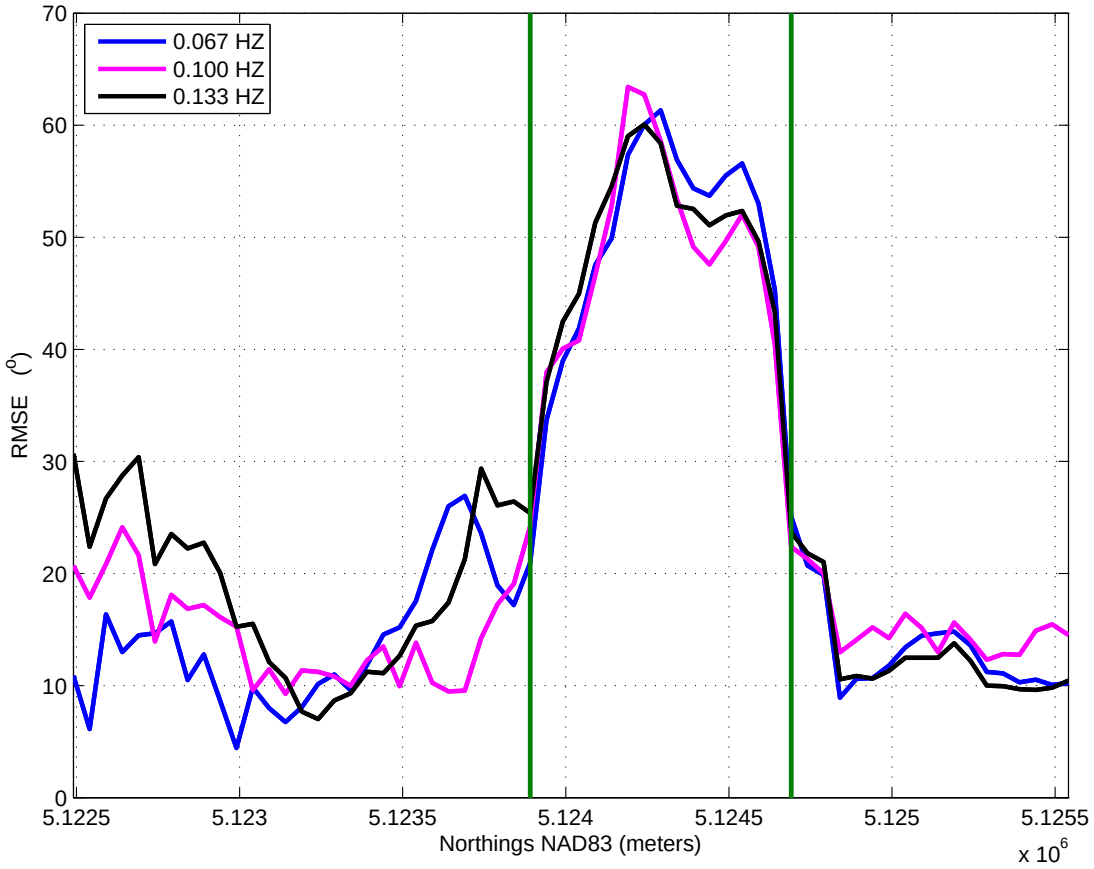

Fig. 4.5: Root mean square error calculated with the SWAN wave-current interaction cases and the Radar 150 meter (3 point) running averaged radar data for 0.067 (blue), 0.100 (magenta), and 0.133 (black) Hz.

Table 4.1: Regression analysis of SWAN and Radar wave direction results. Regression A does not include the region of poor disagreement. Regression B considers the entire transect.

	Regression A		Regression B	
Year Date and Time (PST)	**Slope**	**R^2**	**Slope**	**R^2**
17 16:00	0.70	0.83	0.41	0.36
17 19:00	0.75	0.74	0.31	0.18
17 22:00	0.86	0.78	0.61	0.47
18 01:00	0.53	0.27	0.43	0.31
18 04:00	0.41	0.06	0.30	0.00
18 07:00	0.80	0.78	0.53	0.56
18 13:00	0.87	0.67	0.54	0.32
18 16:00	0.99	0.71	0.63	0.15
18 19:00	0.73	0.78	0.40	0.25
18 22:00	0.68	0.73	0.42	0.47
19 01:00	0.66	0.84	0.45	0.56
19 04:00	0.60	0.67	0.42	0.43
19 07:00	0.87	0.64	0.38	0.06
19 13:00	0.72	0.41	0.46	0.12

the green vertical lines. The results from the regression analysis (slope and R^2 values) are shown in Table 4.1. Here slopes range from 0.43 to 0.99 with a mean R^2 value of 0.64. A second analysis was completed including all of the values along the transect. When the area of poor agreement is included in the analysis slopes range from 0.31 to 0.63 with a mean R^2 value of 0.30. The regression analysis for each case is plotted in Figure 4.6.

4.1.2 Wave Angle Conclusions

SWAN and the radar show good agreement except for the region north of the north jetty. This result is puzzling because over a shoal, such as Peacock Spit, it is expected that radar and SWAN should have good agreement. In this region the SWAN-outputted wave direction follows the bathymetric contours, focusing around the spit. However the gradient in wave direction from northward propagation to normal incidence is very high,

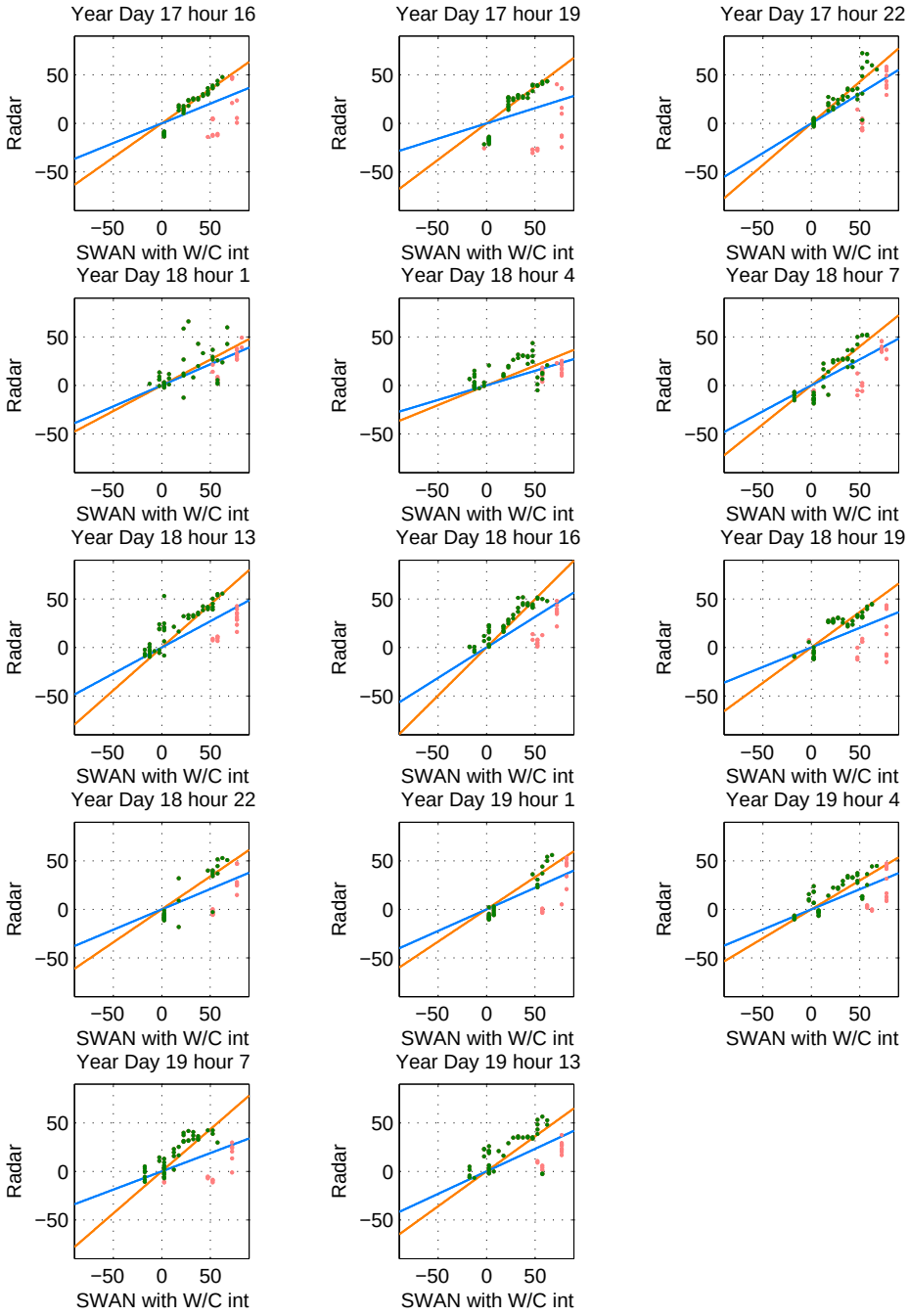

Fig. 4.6: Regression analysis of the 14 SWAN-Radar comparisons. Regression excluding the region of poor disagreement (marigold), Wave angles excluding the points contained within the region of poor disagreement (green), wave directions in the region of poor disagreement (pink), regression including the region of poor disagreement(blue).

requiring a significant amount of refraction between model grid points. The radar is very close to this region, and the wave crests are normal to the radar. This is an ideal vantage point for the radar; hence, the radar observations should be reliable.

Originally, the region of disagreement was thought to have been caused by energy leakage across the north jetty. The model domain was modified to better define the north jetty and ensure it was surface piercing for all tidal levels. This was corrected manually by tracing the contours of the north jetty and replacing the existing depth values with a surface piercing depth. After jetty modification the region of disagreement was equally as pronounced, indicating that energy leakage across the jetty was not the source of the disagreement.

One possible explanation is that the radar is making observations based on current bathymetry. The bathymetry used in SWAN is constant over time, hence would not reflect the recent changes in the bathymetric profile. The along-shore transect includes data from bathymetric surveys collected July of 2006 (Ruggerio, 2005), six months after the radar data collection was completed; however, the survey would not reflect changes in winter and summer profiles. This indicates that there may be changes in the bathymetric contours on the shoal that the model domain does not reflect.

Lastly, the tidal elevation and current fields entered into SWAN were computed by CORIE. Observations were unavailable to validate these current fields, as such, their accuracy is uncertain. However, the SWAN neglecting current cases show similar behavior to the including current cases, indicating that the errors may not be due to wave-current interactions.

SWAN also has a history of difficulty calculating refraction angles greater than 50^o, which occurs in the region of disagreement (Rogers, 2007). Thus, this error could be due to poor calculation of wave refraction around Peacock Spit by SWAN.

4.1.3 Wave Breaking

Wave breaking information was extracted from the raw radar data collected during January 16–19, 2006. A wave breaking proxy is assumed to occur when radar intensity exceeds a defined threshold value. The threshold is defined by the mean image intensity over a geographic region, ± one standard deviation from the mean (Catalan, 2007).

To make comparisons to SWAN of wave breaking, two sites were selected (Figure 4.2). These sites were selected in an effort to isolate locations where depth-limited breaking would be the dominant dissipation, such as an area on a shoal, and where current-induced breaking would be the dominant dissipation, such as in the navigational channel. The first site is located on Peacock Spit (Figure 4.2). This location will be referred to as the "Shoal". The second site is located within the navigational channel, which will be referred to as the "Channel" (Figure 4.2). (There is no wave breaking data available from the radar on year day 16.) At these sites the percentage of breaking waves output from SWAN was used to make comparisons with radar.

Mean wave, still water depth and tidal conditions for both sites are listed in Table 4.2. The conditions reported in the table are SWAN-predictions at one point location within the isolated regions. On the shoal this point is located at Northing 5124090 and Easting 414999. The point location with the channel is Northing 4122490 and Easting 415899. The time series of these conditions is displayed in Figure 4.7. Figure 4.7 and Table 4.2 show the water depth in the channel is twice as deep as on shoal. The mean and maximum wave height, H, on the shoal is comparable to the H in the channel. Tidal current magnitudes are greatest in the channel.

The influence of current on wave conditions was also investigated at each location, shoal and channel. This was evaluated by computing the current direction and comparing to the SWAN-predicted wave direction. The current direction was computed by taking the arctangent of the u and v components to get an angle measurement. Special

Table 4.2: Mean tidal, wave, and depth characteristics at SWAN/radar wave breaking comparison locations.

	Shoal	**Channel**
$U_{magnitude}$ Opposing (m/s)	-0.62	-1.13
$U_{magnitude}$ Following (m/s)	0.46	0.61
H (m)	4.36	3.80
θ (^{o})	51.56	30.9
Depth (m)	9.47	22.46

consideration was given to the sign of u and v to make sure that the current direction was represented correctly. Tidal currents will have the largest effect on the wave conditions when the wave direction is 0 or 180^o to the wave propagation direction (following or opposing, respectively). The opposite is true when the current is +90 or 270^o from the wave direction. This means the current is perpendicular to the wave, and does not affect the wave characteristics. For this analysis, angles are measured counter-clockwise from directly east. To assess the importance of current on the wave conditions at the shoal four cases were selected to compare the wave and current directions, two of which are opposing currents and the other two are following currents.

Shoal

Both radar-observed and SWAN-computed wave breaking is shown in Figure 4.7. The radar and SWAN comparisons of wave breaking on the shoal, visually, indicate good agreement.

The current direction computed at the shoal for the four cases investigated was 173.78^o (yd 17, 19:00), 183.86^o (yd 18, 19:00), 279.13^o (yd 17, 13:00) and 295.97^o (yd 18, 01:00). The first two current directions are from opposing current cases, and both angles represent the current direction almost directly westward. The wave direction for both cases is 62.5^o. The angle between the wave and the current directions are 111.27^o and 113.64^o, resectfully. Both of these angles are close to 90^o, indicating there

is little effect of the current on the wave characteristics on the shoal. For these cases, wave heights increased 1% with the inclusion of currents. The other angles (279.13^o and 64.03^o) investigated occurred on following current cycles. The wave direction on the shoal at these times was 47.5^o and 47.5^o, respectively. The difference between the wave angle and the current angle are 236.64^o and 248.47^o. The difference in wave and current angle is relatively close to 90^o and 270^o. Wave height decreased 1% with the inclusion of currents, indicating that the effect of current is also low in the following current cases.

Channel

The location chosen within the channel is relatively deep (22.46 meters $\pm$ tidal elevation changes). Using the saturated breaking linear relationship $H = \gamma h$, where γ value of 0.73 (the default SWAN value) and h water depth, a 16 meter wave height would be required to have saturated-depth-induced-breaking at this location. As a result, the channel is an optimal location to evaluate current induced breaking. In the channel SWAN does not predict any wave breaking; however, the radar does estimate a percentage of waves breaking. The radar breaking data does not, visually, correspond well to oscillations in H, θ, or tidal cycle. We would expect more breaking when waves are larger or when water depth was less (ebb tide); however, this relationship was not found.

In the channel, the same four cases (as on the shoal) were evaluated to determine the influence of current on wave-characteristics: 192.86^o (yd 17, 19:00), 195.86^o (yd 18, 19:00), 12.65^o (yd 17, 13:00) and 17.13^o (yd 18, 01:00). The first two cases are opposing current conditions, while the last two cases are following current conditions. The wave direction for both the first two cases were 27.5^o, thus the angle between the current and wave direction is 165.36^o and 168.36^o, respectively. Both angle differences are very close to 180^o indicating that current is influential on the wave characteristics and that current

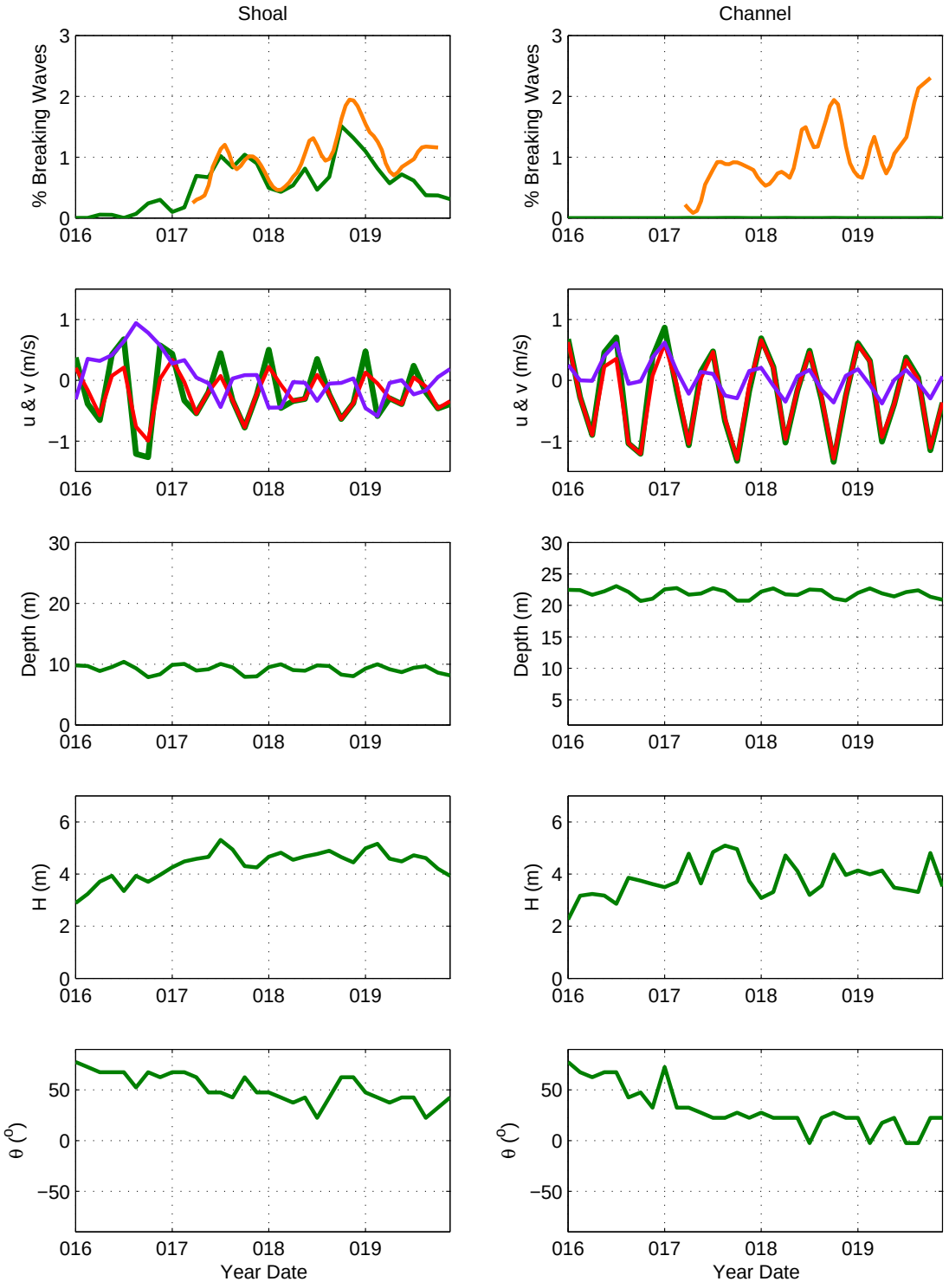

Fig. 4.7: **Top Row:** Percentage of wave breaking on the shoal (left) and in the channel (right) outputted from SWAN (green) and the radar(marigold). **Second Row:** Tidal currents at the shoal and channel locations in $U_{magnitude}$ (green), u (red) and v (purple). **Third Row:** Water depth at each location including tidal adjustments. **Fourth Row:** Wave height. **Fifth Row:** Wave Direction-where the wave is towards. (green)

opposes the direction of wave propagation. Wave height increases 15% for both cases evaluated. The direction of wave propagation for the following current cases (12.65^o (yd 17, 13:00) and 17.13^o (yd 18, 01:00)) is 22.5^o and 27.5^o. The angle difference is 9.84^o and 10.36^o, respectively. The difference in angle between the current and wave direction of both following current cases is close to zero, indicating that the current in the channel is significantly affected by following currents. Wave height decreases 15% for both cases.

4.1.4 Discussion

On the shoal SWAN-predicted and radar-estimated wave breaking compared well. Percent of breaking waves predicted by SWAN did not appear to have a dependence on wave characteristics. The direction of current on the shoal is relatively close to 90^o and 270^o relative to the wave direction, indicating that the wave conditions are minutely effected by the currents. At this location the change in wave height resulting from the inclusion of currents is 1%.

In the channel, SWAN did not predict any wave breaking; however, the radar estimated a similar wave breaking percentage as on the shoal. The current direction, with respect to the wave direction, in the channel was close to 0^o or 180^o indicating the currents are influential on the wave characteristics.

The importance of whitecapping was investigated as an important dissipation mechanism within the domain with respect to steepness limited breaking. Whitecapping is wind-induced breaking that is not related to depth-limited or current-induced breaking. Upon completion of SWAN model simulations for January 16–19, 2007 data set, whitecapping did not make a significant increase in wave breaking in the channel. Alternatively, the addition of whitecapping induced uniform dissipation across the entire domain reducing the breaking dissipation. As a result, whitecapping was not considered

as a significant contributor to steepness limited breaking in the inlet.

4.2 Comparisons of In-situ Data and Model

The USACE placed Acoustic Doppler Profiles (ADP) and Optical Back Scatter Senors (OBS) at three sites at the MCR from August 14–October 1, 1997 (Figure 2.1). The three sites are referred to as B1, B2 and E. B1 is located on top of a dredge deposit mound (Northing 5120568, Easting 409476). B2 is located adjacent to site B1, 0.85 kilometers seaward of the mound (Northing 5120580, Easting 408653). E is located to the north of the navigational inlet and seaward of the north jetty on another dredge deposit mound (Northing 5122158, Easting 413509)(ERDC).

The ADP's reported wave conditions that include wave height, H, and peak wave direction, θ_p, every three hours. So far, six days have been used to compare with SWAN model results. We are only showing comparisons with SWAN simulations neglecting wave-current interaction. The root mean square difference of SWAN-neglecting-and-including-wave-current-interaction simulations at these locations is on the order of 10 percent; as such, wave-current interaction was not considered to be a dominant factor. Work et. al. (1997) found similar results in Pensacola, Florida where the instrument locations were placed to far away from the inlet to observe the effects of tidal currents on the wave field.

The data set was analyzed from August 21, 1997 at 0:00 to August 26, 1997 at 23:00 PST (48 cases–year days: 233-238). Wave conditions are shown in Figure 3.1. During the study period wave heights ranged from 0.86–2.61 meters, wave periods ranged from 4-8 seconds and waves were going to the east and northeast. Year day 235, buoy information was unavailable, represented by discontinuities in the time series of wave conditions (Figure 3.1) and SWAN-computed results (Figures 4.8 and 4.9).

For these simulations, the buoy was located relatively close to shore (Northing

5114737, Easting 407983). As a result the model domain size was reduced (Section 2.2.2). A full two-dimensional spectrum was unavailable from the buoy; as such, the energy spectrum was represented by the significant wave height, peak wave period and mean wave direction reported by the buoy (NDBC 46029). A Jonswap spectrum (Hasselman, 1973) was assumed with a peak enhancement parameter of 3.3 and a $\cos^m(\theta - \theta_{peak})$ distribution, where $m = 30$, both default values. Sensitivity to spectral and directional width still needs to be addressed.

4.2.1 Results

A sample case was selected to show H over the model domain, as well as the location of in-situ observations (Figure 4.8). Figure 4.8 shows H computed by SWAN and observed by the in-situ measurements, and the offshore buoy is shown for reference. Both sites B1 and B2 are 5.8 kilometers to the north of the buoy location. Site E is 7.4 kilometers north of the buoy location.

Both sites B1 and B2 are close to the seaward edge of the domain, resulting in SWAN predictions that do not differ much from the buoy observations, although the buoy is 5.8 kilometers to the south of the in-situ locations. At B1 both SWAN, buoy and in-situ observations agree very well. This result is expected since the in-situ observations are very close to the seaward edge of the domain. Here the root mean square error (RMSE) of the SWAN-predicted and in-situ results is 0.26 m (Table 4.3). As expected, wave height at E (the closest to shore) differs from buoy measurements. This difference in H results from focusing and shoaling effects on the bathymetry. Model results at E also agree very well with the in-situ observations. RMSE of SWAN-results and in-situ observations are listed on Table 4.3. At B2 the in-situ observations are less than the SWAN-computed and buoy-observed results. RMSE of H at B2 is 0.5 meters, double the RMSE at B1.

Table 4.3: RMSE computations of SWAN, neglecting current, and the in-situ measurements of wave height and wave direction. Evaluating wave characteristics and tidal currents.

Site	B1	B2	E
H (m)	0.26	0.50	0.19
θ_p (^{o})	38.19	–	33.00

On year day 236, the buoy and in-situ observations indicate an increase in wave height (Figure 4.8). SWAN also predicts the same trend; however, under predicts the value of H at both sites. SWAN computes wave heights that are slightly greater than in-situ observations for the rest of the time series. The over prediction is on the order of centimeters. Overall, SWAN shows good agreement in the predictions of H.

To make comparisons of wave direction, wave direction is referred to in the context of where the wave is moving toward (+90 is northward wave propagation). In-situ observations are unavailable at site B2 during the study period. Sites B1, B2 and E show good buoy agreement (Figure 4.9). Visually, SWAN tends to under predict northward (+) propagating waves and over predicts southward propagating waves when compared to the in-situ observations. SWAN predictions at B1 and E indicate a 26^o mean shift in wave angle to the south in comparison to the insitu observations. Although, visually similar trends in wave direction occur, the offset remains unexplained.

4.2.2 Discussion

SWAN, buoy and in-situ observations of wave height at B1 and E agree well, with the largest RMSE of 0.26 meters. Agreement of B2 is less satisfactory, with an RMSE error of 0.5 meters. The disagreement in wave height between SWAN-predicted and in-situ-observations at B2 could be related to the seaward boundary of the domain. Site B1 is 825 meters away from the seaward edge of the domain. Along the boundary we assume that wave energy is constant. As a result, SWAN would be unable to predict variability

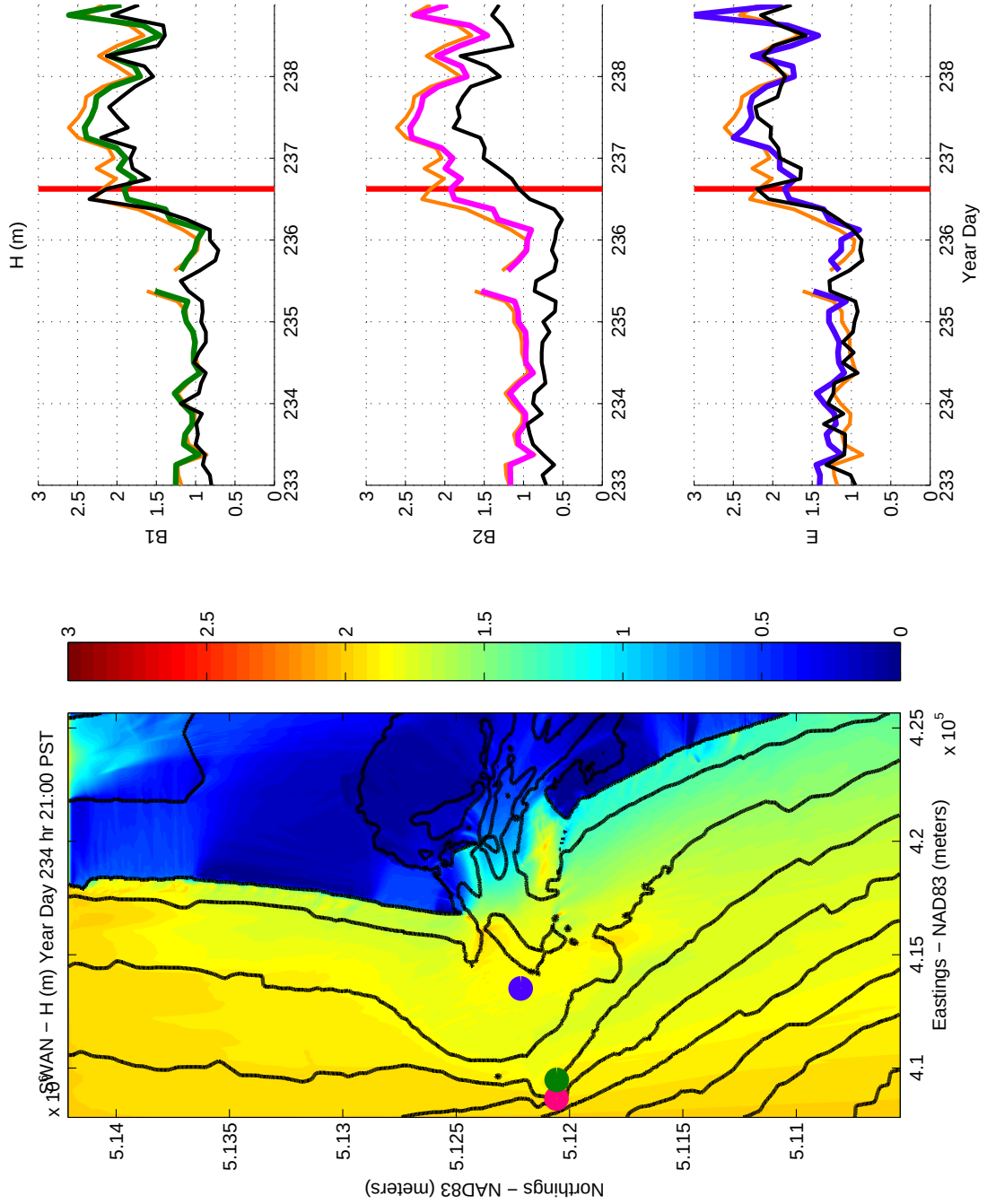

Fig. 4.8: **Left:** Wave height over the model domain, with sites B1 (green), B2 (magenta) and E (purple) indicated. **Right:** Wave height over the study period at sites B1 (top), B2 (middle) and E (bottom). The black line represents the in-situ observation at each location. The green, magenta and purple lines are indicative of the SWAN observations. The red line indicates the location in the times series where the wave height plot (left) occurred. The marigold line is depreciative of values reported by buoy 46029.

in wave energy along the boundary. However, if wave variability were likely to occur along the edge of the domain, in-situ/model comparisons at B1 (850 meters shoreward of B2) would also show this disagreement.

Another possible source of error is bathymetry. SWAN simulations were completed with a model domain composed of bathymetric surveys from 2003-2004. We assume that the bathymetry in 2003–2004 is representative of 1997 bathymetry. Significant bathymetric changes could be responsible for the disagreement in wave height predictions and observations. However, ultimately the source of disagreement at B2 is unexplained.

SWAN-computed results of wave angle reflect a mean 26^o shift southward when compared to insitu-observations. The cause in the southward shift in wave angle is unknown. Otherwise SWAN predicts similar trends to the in-situ observations.

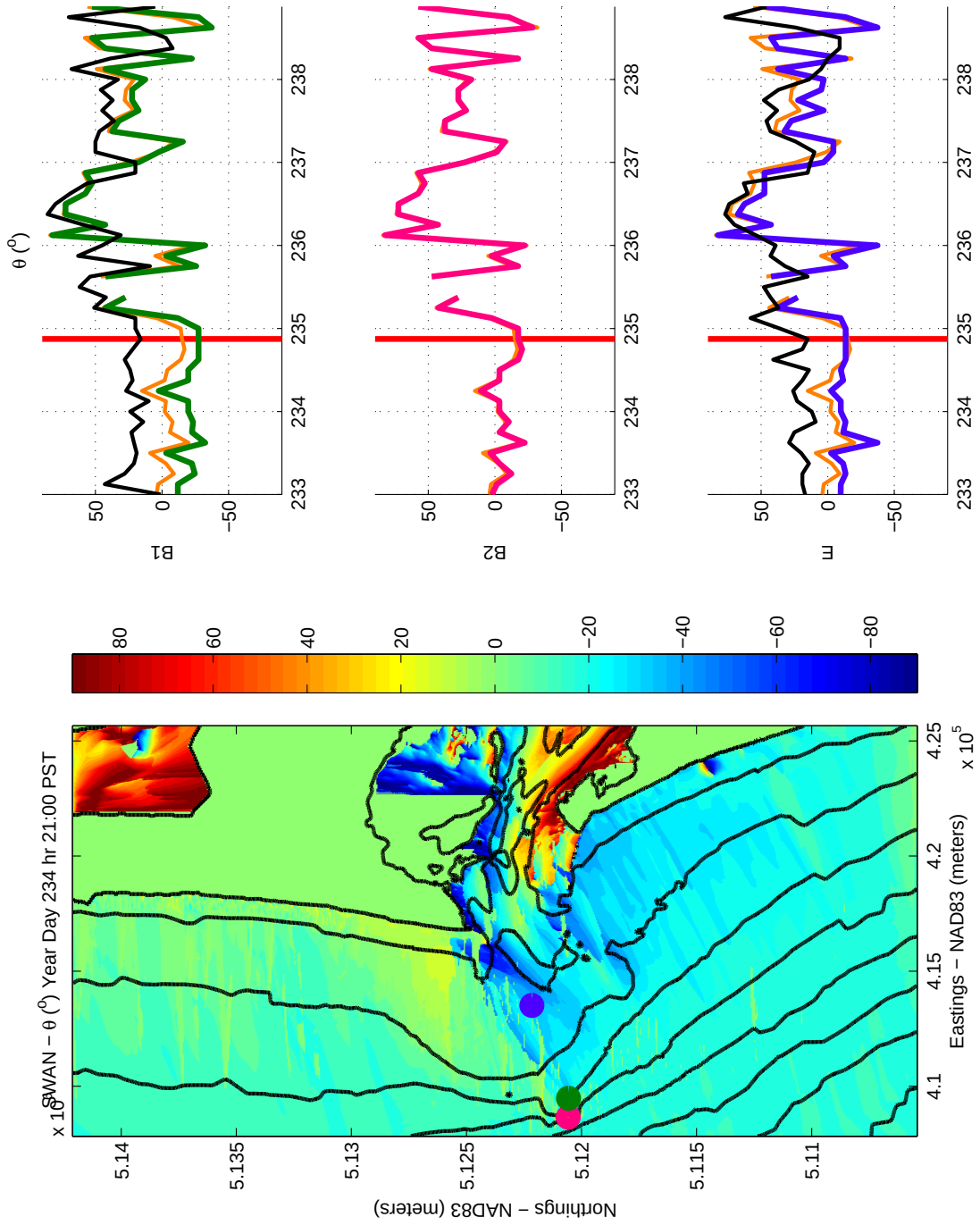

Fig. 4.9: **Left:** Wave direction (θ) over the model domain, with sites B1 (green), B2 (magenta) and E (purple) indicated. **Right:** Wave height over the study period at sites B1 (top), B2 (middle) and E (bottom). The black line represents the in-situ observation at each location. The green, magenta and purple lines are indicative of the SWAN observations. The red line indicates the location in the times series where the wave direction plot (left) occurred. The marigold line is depreciative of values reported by buoy 46029.

5. CONCLUSIONS

This study was designed to evaluate the importance of wave-current interaction at the MCR with a two dimensional wave propagation model, SWAN (Simulating WAves Neashore), as well as validate the predictions of SWAN using remote sensing and in-situ observations (Booij, 1999). SWAN simulations were compared to remote sensing observations of wave direction and wave breaking at the MCR. Additionally, SWAN-computed wave height and direction are compared to in-situ observations for validation at the MCR.

SWAN indicates wave-current interaction at the mouth of the Columbia River is an important factor during January 16–19, 2006. Maximum opposing currents were 2.03 m/s resulting in a maximum increase in wave height, H, of 1.88 meters and a maximum decrease in wave length, L, of 74.54 meters. Maximum following currents are 1.38 m/s, generating a maximum decrease in H of 0.72 meters and increase in maximum L of 31.51 meters. This indicates that ΔH and ΔL are 60.6 and 57.7 percent greater for opposing currents than following currents. The magnitude of maximum opposing currents is greater than the following currents by 31.6 percent. These results agree with Enfield (1974) who documented following currents were on average 60 percent of opposing currents. As a result, the influence of following currents on the wave field was not as pronounced in comparison to opposing currents.

SWAN and remote sensing observations of wave direction and wave breaking were compared for 14 cases. Wave direction results from both SWAN and radar indicate good agreement in the navigational channel and Benson Beach. However, wave direction estimates do not agree well over Peacock Spit. In this region the wave propagation

direction turns sharply from obliquely north to normally incident. Both SWAN and the radar report this change in wave direction. This change in wave angle requires significant wave turning. SWAN is known for having difficulty with refraction of angles larger than 50^o (Rogers, 2007). An additional source of error could be bathymetric changes not reflected in the model domain.

The percentage of wave breaking comparisons of SWAN with radar show good agreement on the shoal, where depth-limited breaking is the dominant dissipation mechanism. However, SWAN and radar do not agree when steepness-limited breaking is the dominant dissipation mechanism. Wave breaking and in the channel over the shoal appeared to have some weak dependence on wave angle and height. The difference in wave and current angles indicated that the influence of current on wave characteristics in the navigational channel was high; however, the shoal did not show the same dependence on current as expected.

In-situ observations collected on August 21–26, 1997 at sites B1, B2 and E were compared to SWAN-computed wave height and wave direction. SWAN compared well to in-situ observations of wave height. The largest root mean square error (RMSE), 0.5 meters, occurring at B2. In-situ observations of wave direction were compared to SWAN-predicted wave direction. The comparison showed good agreement. SWAN was used to evaluate the importance of wave-current interaction at these observation locations. Root mean square difference between including and neglecting wave-current interaction was on the order of 10 percent indicating wave-current interaction was not a dominant factor in the wave characteristic during this period at these locations.

SWAN has demonstrated the importance of wave-current interaction as well as proving to be a valuable predictive tool when compared to remote sensing and insitu observations. SWAN does indicate some limitations when considering steepness limited breaking as well as and high angles of refraction.

6. BIBLIOGRAPHY

Baptista, A. M., Zhang, Y., Chawla, A., Zulauf, M., Seaton, C., Myers, E. P., Kindle, J., Wilkin, M., Burla, M., Turner, P. J., (2005). A cross-scale model for 3D baroclinic circulation in estuary-plume-shelf systems: II. Application to the Columbia River. *Continental Shelf Research.* 25, 935–972.

Battjes, J. A., Janssen, J. P. F. M., (1978). Energy loss and set–up due to breaking of random waves. *16th International Conference of Coastal Engineering*, 32, 569–587.

Booij, N., Ris, R.C., Holthuijsen, L. H. (1999). A third-generation wave model for coastal regions 1. Model description and validation. *Journal of Geophysical Research*, 104, 7649-7666.

Chawla, A., Kirby, J. T., (2002). Monochromatic and random wave breaking. *Journal of Geophysical Research*, 107(C7).

Chen, W., Panchang, V., Demirbilek, Z., On the modeling of wave–current interaction using the elliptic mild–slope wave equation. *Ocean Engineering*, 32, 2135–2164.

Enfield, B. D. Prediction of Hazardous Columbia River Bar Conditions. 1974.

Gonzales, F. I (1984), A case Study of Wave-Current-Bathymetry Interactions at the Columbia River Entrance, *Journal of Physical Oceanography*, 1065-1067.

Hasselmann, K. et. al. (1973). Measurements of wind-wave growth and swell decay druing the Joint North Sea Wave Project (JONSWAP), Deutsche Hydrographische Zeitschrift, Hamburg,Reihe A (8^o), No 12,95 pp.

Holthuijsen, L. H., Herman, A., Booji, N. (2003). Phase-decoupled refraction-diffraction for spectral wave models. *Coastal Engineering*, 49, 291-305.

Lin, W., Sanford, L. P., Suttles, S. E. (2002). Wave measurement and modeling in Chesapeake Bay. *Continental Shelf Research*,22, 2673-2686.

Mialsen, D. R., Moritz, H. R., McKillip, D. J., (2006). Potential physical impacts of a littoral drift restoration project–Mouth of the Columbia R., USA. *Coastal Engineering*, vol 2, 1964–1976.

Moritz, H. R., Gelfenbaum, G. R., Kaminsky, G. M., Kraus, N. C., Ruggerio, Oltman-Shay, J., McKillip, D. J. Implementing Regional Sediment Management To Sustain Navigation at an Energetic Tidal Inlet, 2007.

Osuna, P., Monbaliu, J., (2004). Wave–current interaction in the Southern North Sea. *Journal of Marine Systems*, 52, 65–87.

Park, K. Y., Brothwick, A. G. L., Cho, Y. S., (2006). Two–dimensional wave–current interaction with a locally enriched quadtree grid system. *Ocean Engineering*, 33, 247–263.

Plant, N. G. (2007). Estimation of wave celerity from nearshore video and radar platforms. (In Press)

Resio, D. T., (1987). Shallow-=water waves. I: Theory. *Journal of Waterway, Port, Coast and Ocean Engineering*, ASCE, 114(1), 50–65.

Rogers, E. R., Kaihatu, J. M., Hsu, L., Janssen, R. E., Holland, K. T. (2007). Forecasting and hindcasting waves with SWAN model in the Southern California Bight. *Coastal Engineering*, 54, 1-15.

Rogers, W. E., Hwang, P. A., Wang, D. W., (2002). Investigation of Wave Growth and Decay in the SWAN Model: Three Regional–Scale Applications. *Journal of Physical Oceanography*, 33, 366–389.

Ruggerio, P., Kaminsky, G. M., Gelfenbaum, G, M., Voigt, B. (2005). Seasonal to interannual morphodynamics along a high-energy dissipative littoral cell. *Journal of Coastal Research*, 21(3), 553-578.

Ruggerio, P., Kaminsky, G. M., Komar, P. D., McDougal, W. G., (1997). Extreme waves and coastal erosion in the Pacific Northwest. *Wave Measurements and Analysis, Proceedings of the 3_{rd} International Symposium, Waves '97*, 947–961.

Saeed, M., Gayer, G., Günther, H., Shafieefar, M., (2005). Application of third generation shallow water wave models in a tidal environment. *Ocean Dynamics*, 55, 10–27.

Schneggenburger, C., Günther, H., Rosenthal, W., (2000). Spectral wave modelling with non–linear dissipation: validation and applications in coastal tidal environment. *Coastal Engineering*, 41, 201–235.

Smith, S. J., Smith, J. M., (2001). Numerical Modeling of Waves at Ponce de Leon Inlet, Florida. *Journal of Waterway, Port, Coastal and Ocean Engineering*, May/June, 176–183.

Wilma, D (2006). Graveyard of the Pacific: Shipwrecks on the Washington Coast. The Online Encyclopedia of Washington State History. *www.historylink.org/essays/output.cfm?file*
7936

Work, P. A., Kaihatu, J. M., (1997). Wave Transformation at Pensacola Pass, Florida. *Journal of Waterway, Port, Coastal, and Ocean Engineering*, 123(6),314–321.

Work, P. A., Pehrenbacher, F., Vougaris, G., (2004). Nearshore Impacts of Dredging for Beach Nourishment. *Journal of Waterway, Port, Coastal and Ocean Engineering*, 130(6), 303–311.

Zhang, Y., Baptista, A. M., Myers, E. P., (2004). A cross-scale model for 3D baroclinic circulation in estuary-plume-shelf systems: I. Formulation and skill assessment. *Continental Shelf Research*, 24, 2187–2214.